Manuscript prepared for Clim. Past
with version 2014/07/29 7.12 Copernicus papers of the LaTeX class copernicus.cls.
Date: 8 September 2014

arXiv:1409.1880v1 [astro-ph.EP] 5 Sep 2014

Radiative forcings for 28 potential Archean greenhouse gases

B. Byrne and C. Goldblatt

School of Earth and Ocean Sciences, University of Victoria, Victoria, BC, Canada

Correspondence to: B. Byrne (bbyrne@uvic.ca)

Abstract. Despite reduced insolation in the late Archean, evidence suggests a warm climate which was likely sustained by a stronger greenhouse effect, the so-called Faint Young Sun Problem (FYSP). CO_2 and CH_4 are generally thought to be the mainstays of this enhanced greenhouse, though many other gases have been proposed. We present high accuracy radiative forcings for CO_2, CH_4 and 26 other gases, performing the radiative transfer calculations at line-by-line resolution and using HITRAN 2012 line data for background pressures of 0.5, 1, and 2 bar of atmospheric N_2. For CO_2 to resolve the FYSP alone at 2.8 Gyr BP (80 % of present solar luminosity), 0.32 bar is needed with 0.5 bar of atmospheric N_2, 0.20 bar with 1 bar of atmospheric N_2, or 0.11 bar with 2 bar of atmospheric N_2. For CH_4, we find that near-infrared absorption is much stronger than previously thought, arising from updates to the HITRAN database. CH_4 radiative forcing peaks at 10.3, 9, or 8.3 $\mathrm{W\,m^{-2}}$ for background pressures of 0.5, 1 or 2 bar, likely limiting the utility of CH_4 for warming the Archean. For the other 26 HITRAN gases, radiative forcings of up to a few to 10 $\mathrm{W\,m^{-2}}$ are obtained from concentrations of 0.1–1 ppmv for many gases. For the 20 strongest gases, we calculate the reduction in radiative forcing due to overlap. We also tabulate the modern sources, sinks, concentrations and lifetimes of these gases and summaries the literature on Archean sources and concentrations. We recommend the forcings provided here be used both as a first reference for which gases are likely good greenhouse gases, and as a standard set of calculations for validation of radiative forcing calculations for the Archean.

1 Introduction

The standard stellar model predicts that the luminosity of a star increases over its main-sequence lifetime (Gough, 1981). Therefore, the sun is 30 % brighter now than it was when the solar system formed. Despite a dimmer sun during the Archean (3.8–2.5 Gyr BP), geologic evidence suggests surface temperatures similar to today (Donn et al., 1965): This apparent paradox is known as the faint young sun problem (FYSP). To reconcile this, Earth must have had a lower albedo and/or a stronger greenhouse effect in the past. In this work we focus on a stronger greenhouse effect, which is thought to be the primary cause of the warming (Goldblatt and Zahnle, 2011b; Wolf and Toon, 2013). We focus on the late Archean with a solar constant of $0.8\,S_0$, resulting in an reduction of $\approx$50 $\mathrm{W\,m^{-2}}$ of insolation.

NH_3 was proposed as a solution to the FYSP soon after the problem was posed (Sagan and Mullen, 1972). NH_3 is a strong greenhouse gas and concentrations of 10 ppmv could have warmed the Archean surface by 12–15 K (Kuhn and Atreya, 1979). At the time NH_3 was proposed as a solution, it was thought that the early Earth was strongly reducing such that NH_3 could have built up to significant atmospheric concentrations. However, the Archean atmosphere is now thought to have been only mildly reducing. NH_3 would likely have photo-dissociated rapidly without UV protection (Kuhn and Atreya, 1979; Kasting, 1982). Furthermore, NH_3 is highly soluble and would have been susceptible to rain-out. Therefore, sustaining atmospheric concentrations of NH_3 at which there is significant absorption may not be as easy as originally thought. Considering the destruction of NH_3 by photolysis, Kasting (1982) found that concentrations as high as 10 ppbv could plausibly be attained by biotic sources. If NH_3 were shielded from UV radiation (by a possible organic haze layer) larger concentrations could be sustained, though concentrations above 1 ppbv seem unlikely (Pavlov et al., 2000).

The most obvious resolution to the FYSP would be higher CO_2 partial pressures. It is believed that the inorganic carbon cycle provides a strong feedback mechanism which regulates the Earth's temperature over geologic timescales (Walker et al., 1981). The rate of silicate weathering (a sink of atmospheric CO_2) is a function of surface temperature which depends on the carbon dioxide partial pressure through the greenhouse effect. Therefore, reduced insolation requires

higher atmospheric CO_2 concentrations to regulate the surface temperature and balance the sources (volcanoes) and sinks of atmospheric CO_2. However, geological constraints have been proposed which limit atmospheric CO_2 to levels below those required to keep the early Earth warm (Sheldon, 2006; Driese et al., 2011). Sheldon (2006) used a model based on the mass balance of weathering paleosols and find CO_2 partial pressures between 0.0028-0.026 bar at 2.2 Gyr ago. Driese et al. (2011) use the same method and find CO_2 partial pressures between 0.003 and 0.02 bar at 2.69 Gyr ago. However, these constraints are not uniformly accepted (Kasting, 2013).

Other greenhouse gases likely played an important role in the early Earth's energy budget. Most of the focus has been applied to CH_4 as there are good reasons to expect higher concentrations during the Archean (Zahnle, 1986; Kiehl and Dickinson, 1987; Pavlov et al., 2000; Haqq-Misra et al., 2008; Wolf and Toon, 2013). The Archean atmosphere was nearly anoxic, with very low levels of O_2, which would have increased the photochemical lifetime of methane from 10-12 years today to 1000-10,000 years (Kasting, 2005). The concentration of methane in the Archean is not well constrained but Kasting (2005) suggests that 1-10 ppmv could have been sustained from abiotic sources and up to 1000 ppmv could have been sustained by methanogens. Redox balance models suggest concentrations $\approx$100 ppmv (Goldblatt et al., 2006). Recent GCM studies have found that reasonably warm climates can be sustained within the bounds of the CO_2 constraints if the greenhouse is supplemented with elevated CH_4 concentrations (Wolf and Toon, 2013; Charnay et al., 2013). Wolf and Toon (2013) find modern day surface temperature with 0.02 bar of CO_2 and 1000 ppmv of CH_4 with 80 % of present solar luminosity.

Other potential greenhouse gases which have been examined include hydrocarbons (Haqq-Misra et al., 2008), N_2O (Buick, 2007; Roberson et al., 2011), and OCS (Ueno et al., 2009; Hattori et al., 2011). C_2H_6 has been suggested to have been radiatively important in the Archean because it can form in significant concentrations from the photolysis of CH_4 at high partial pressures (Haqq-Misra et al., 2008). Haqq-Misra et al. (2008) find that 1 ppmv of C_2H_6 could increase the surface temp by $\approx$3 K, and 10 ppmv by $\approx$10 K. However, C_2H_6 is formed along with other organic compounds which form an organic haze. This organic haze is thought to provide a strong anti-greenhouse effect which limits the utility of C_2H_6 to warm the climate when produced in this manner.

Elevated OCS concentrations were proposed by Ueno et al. (2009) to explain the negative $\Delta^{33}S$ observed in the Archean sulfate deposits. However, Hattori et al. (2011) report measurements of ultraviolet OCS absorption cross-sections and find that OCS photolysis does not cause large mass independent fractionation in $\Delta^{33}S$ and is therefore not the source of the signatures seen in the geologic record.

Buick (2007) proposed that large amounts of N_2O could have been produced in the Proterozoic due to bacterial denitrification in copper depleted water, because copper is needed in the enzymatic production of N_2 from N_2O (which is the last step of denitrification). Roberson et al. (2011) find that increasing N_2O from 0.3 ppmv to 30 ppmv warms surface temperatures by ≈ 8 K. However, Roberson et al. (2011) also show that N_2O would be rapidly photo-dissociated if O_2 levels were lower than 0.1 PAL and that N_2O was unlikely to have been produced at radiatively important levels at O_2 levels below this.

Examining the Archean greenhouse involves calculating the radiative effects of greenhouse gases over concentration ranges never before examined. Typically, one time calculations are performed with no standard set of radiative forcings available for comparison. The absence of a standard set of forcings has led to errors going undetected. For example, the warming exerted by CH_4 was significantly overestimated by Pavlov et al. (2000) due to an error in the numbering of spectral intervals (Haqq-Misra et al., 2008) which went undetected for several years.

In previous work, greenhouse gas warming has typically been quantified in terms of the equilibrium surface temperature achieved by running a one-dimensional Radiative-Convective Model (RCM). This metric is sensitive to how climate feedbacks are parametrized in the model and to imposed boundary conditions (e.g., background greenhouse gas concentrations). This makes comparisons between studies and greenhouse gases difficult. It is desirable to document the strengths and relative efficiencies of different greenhouse gases at warming the Archean climate. However, this is near impossible using the literature presently available.

In this study, we use radiative forcing to quantify changes in the energy budget from changes in greenhouse gas concentrations for a wide variety of greenhouse gases. We define radiative forcing as the change in the net flux of radiation at the tropopause due to a change in greenhouse gas concentration with no climate feedbacks. The great utility of radiative forcing is that, to first order, it can be related through a linear relationship to global mean temperature change at the surface (Hansen et al., 2005). It therefore provides a simple and informative metric for understanding perturbations to the energy budget. Furthermore, since radiative forcing is independent of climate response, we get general results which are not affected by uncertainties in the climate response. Radiative forcing has been used extensively to study anthropogenic climate change (IPCC, 2013).

Imposed model boundary conditions significantly affect the warming provided by a greenhouse gas. Boundary conditions that typically vary between studies include: atmospheric pressure, CO_2 concentrations, and CH_4 concentrations. The discrepancies in boundary conditions between studies develop from the poorly constrained climatology of the early Earth. In this work, we examine the sensitivity of radiative forcings to variable boundary conditions.

The atmospheric pressure of the Archean is poorly constrained but there are good theoretical arguments to think it

was different from today. For one, the atmosphere is 21 % O_2 by volume today, whereas there was very little oxygen in the Archean atmosphere. Furthermore, there are strong theoretical arguments that suggest that the atmospheric nitrogen inventory was different: large nitrogen inventories exist in the mantle and continents, which are not primordial and must have ultimately come from the atmosphere (Goldblatt et al., 2009; Johnson and Goldblatt, 2014). Constraints on the pressure range have recently been proposed, from raindrop imprints (Som et al., 2012) – though this has been challenged (Kavanagh and Goldblatt, 2013), and from noble gas systematics (0.7-1.1 bar, Marty et al., 2013).

Atmospheric pressure affects the energy budget in two ways. (1) Increasing pressure increases the moist adiabatic lapse rate. The moist adiabatic lapse rate is a function of the saturation mixing ratio of water vapour. The saturation vapour pressure is independent of pressure. Increasing pressure means there is more dry air to absorb the latent heat released by condensation, making the moist adiabatic lapse rate larger (closer to the dry adiabatic lapse rate). (2) As the pressure increases, collisions between molecules become more frequent. This results in a broadening of the absorption lines over a larger frequency range. This phenomena is called pressure broadening and generally causes more absorption (Goody and Yung, 1995).

Changes to the concentrations of CO_2 and CH_4 will affect the strength of other greenhouse gases. When multiple gases absorb radiation at the same frequencies, the total absorption is less than the sum of the absorption that each gas contributes in isolation. This difference is known as overlap. It occurs because the absorption is distributed between the gases, so in effect there is less radiation available for each gas to absorb.

In this paper, we present calculations of radiative forcings for CO_2, CH_4 and 26 other gases contained in the HIgh-resolution TRANsmission (HITRAN) molecular database for atmospheres with 0.5 bar, 1 bar, and 2 bar of N_2. We aim to provide a complete set of radiative forcing and overlap calculations which can be used as a standard for comparisons. We provide CO_2 and CH_4 radiative forcings over large ranges in concentration, and compare our results with calculations in the literature. For the other 26 HITRAN gases, the HITRAN absorption data is compared with measured cross-sections and discrepancies are documented. Radiative forcings are calculated over a concentrations range of 10 ppbv to 10 ppmv. The sensitivites of the radiative forcings to atmospheric pressure and overlapping absorption with other gases are examined, and our results are compared with results from the literature.

This paper is organized as follows. In section 2, we describe our general methods, evaluation of the spectral data and the atmospheric profile we use. In section 3, we examine the radiative forcings due to CO_2 and CH_4 and examine how our results compare with previous calculations. In section 4, we provide radiative forcings for 26 other gases from the HITRAN database and examine the sensitivity of these results to atmospheric parameters.

2 Methods

2.1 Overview

We calculate absorption cross-sections from HITRAN line parameters and compare our results with measured cross-sections. We develop a single-column atmospheric profile based on constraints of the Archean atmosphere. With this profile, we perform radiative forcing calculations for CO_2, CH_4 and 26 other HITRAN gases. Gas amounts are given in abundances, a, relative to the modern atmosphere (1 bar, molecular weight of 28.97 g/moles, total moles (n_0) of $\approx 1.8\times10^{20}$). Thus $a = n_{gas}/n_0$. As an example, an abundance of 1 for CO_2 contains the same number of moles as the modern atmosphere but would give a surface pressure larger than 1 bar because of the higher molecular weight. For our experiments we add gas abundances to background N_2 partial pressure, increasing the atmospheric pressure.

2.2 Spectra

Line parameters are taken from the HITRAN 2012 database (Rothman et al., 2013). We use the LBLABC code, written by David Crisp, to calculate cross-sections from the line date. Line parameters have a significant advantage over measured absorption cross-sections, in that, absorption can be calculated explicitly as a function of temperature and pressure. The strength of absorption lines is a function of temperature and shape is a function of pressure. Neglecting these dependencies can result in significant errors in radiative transfer calculations.

There are, however, some limitations to using HITRAN data. Rothman et al. (2009) explains that the number of transitions included in the database is limited by: (1) a reasonable minimum cutoff in absorption intensity (based on the sensitivity of instruments that observe absorption over extreme terrestrial atmospheric path lengths), (2) lack of sufficient experimental data, or (3) lack of calculated transitions. The molecules for which data are included in the line-by-line portion of HITRAN are mostly composed of small numbers of atoms and have low molecular weights. Large polyatomic molecules have many normal modes of vibration and have fundamentals at very low wavenumbers (Rothman et al., 2009). This makes it difficult to experimentally isolate individual lines of large molecules, so that a complete set of line parameters for these molecules is impossible to obtain.

Computed cross-sections are compared to measured cross-sections from the Pacific Northwest National Laboratory (PNNL) database (Sharpe et al., 2004) for the strongest HITRAN gases (Fig. 1). Where differences exist, it is not straight forward to say which is in error (for example, potential problems with measurements include contamination

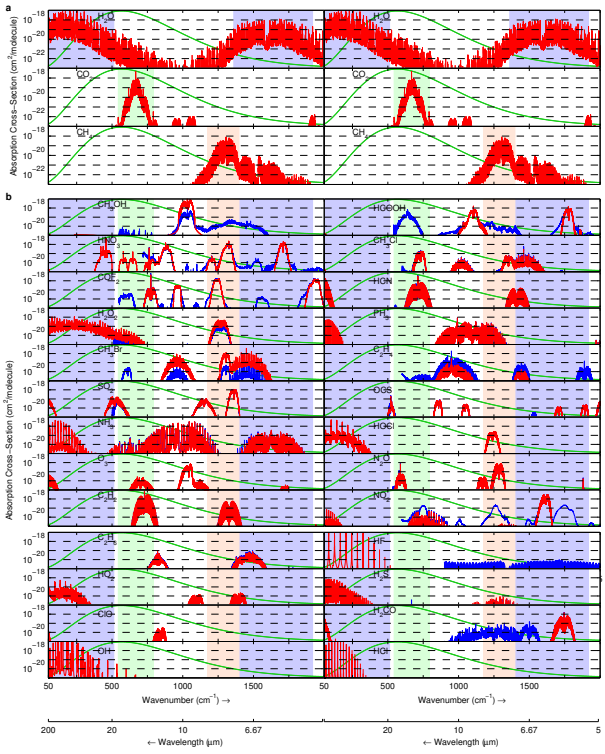

Figure 1. *Absorption cross-sections.* Absorption cross-sections of (a) H_2O, CO_2, and CH_4 and (b) potential early Earth trace gases. Cross-sections are calculated from HITRAN line data (red) and measured from the PNNL database (blue) at 1013 hPa and 278 K. The gases are ordered from strongest to weakest based on the analysis in section 3.3 (Fig. 10) in columns from top left to bottom right. Colored shaded areas show wavenumbers at which absorption is strongest for H_2O (blue), CO_2 (green), and CH_4 (red). The green curve shows the shape of the blackbody emissions from a 289 K blackbody.

of samples). Hence we simply note any discrepancy and do our best to note the consequences of these. The largest abundance of the trace gases examined in this work is 10^{-5}, at this abundance only absorption cross-section greater than $\approx 5 \times 10^{-21}$ cm^2 absorb strongly over the depth of the atmosphere.

The similarities and differences between the cross-sections for each gas are:

- CH_3OH: The HITRAN line data covers the range of 975–1075 cm^{-1}. In that range the HITRAN cross-sections are an order of magnitude larger than the PNNL cross-sections. Therefore, the PNNL data suggests the abundances should be an order of magnitude larger to obtain the same forcings as the HITRAN data. PNNL cross-sections indicate that there is missing HITRAN line data over the range 1075–1575 cm^{-1} with peaks of $\approx 5 \times 10^{-20}$ cm^2, which would be optically thick for abundances $\geq 10^{-6}$. There is also missing HITRAN data at 550–750 cm^{-1} with peaks of $\approx 5 \times 10^{-21}$ cm^2, which would be optically thick for abundances $\geq 10^{-5}$.

- HNO_3: The HITRAN data covers the range of 550–950 cm^{-1}, 1150–1400 cm^{-1}, and 1650–1750 cm^{-1}. Over this range, HITRAN and PNNL data agree well except between 725-825 cm^{-1} where the PNNL cross-sections are larger (relevant for abundances of $\geq 5 \times 10^{-7}$). PNNL cross-sections indicate that there is significant missing HITRAN line data in the ranges 1000–1150 cm^{-1}, 1400–1650 cm^{-1}, and 1750–2000 cm^{-1}, which would be optically thick for abundances $\geq 5 \times 10^{-6}$.

- COF_2: The HITRAN cross-sections cover the range of 725–825 cm^{-1}, 950–1000 cm^{-1}, 1175–1300 cm^{-1}, and 1850–2000 cm^{-1}. The PNNL and HITRAN cross-sections agree over this range. HITRAN is missing bands around 650 and 1600 cm^{-1} with peaks of $\approx 10^{-20}$ cm^2, which would be optically thick for abundances $\geq 5 \times 10^{-6}$. Additionally, wings of 950–1000 cm^{-1}, 1175–1300 cm^{-1}, and 1850–2000 cm^{-1} bands appear missing in HITRAN, relevant at similar abundances.

- H_2O_2: Above 500 cm^{-1}, the HITRAN and PNNL cross-sections cover the same wavenumber range. Over this range, HITRAN cross-sections are about twice the value of the PNNL cross-sections. Therefore, the PNNL

data suggests the abundances should be about twice those of the HITRAN data to obtain the same forcings.

– CH_3Br: HITRAN cross-sections are over an order of magnitude greater than the PNNL cross-sections. Therefore, the PNNL data suggests the abundances should be ≈ 13 times those of the HITRAN data to obtain the same forcings. The PNNL cross-sections indicate missing HITRAN line data over the range of 575–650 cm^{-1} with peaks of $\approx 10^{-20}\,\mathrm{cm}^2$, which would be optically thick for abundances $\geq 5 \times 10^{-6}$.

– SO_2: The HITRAN and PNNL cross-sections agree well except between 550–550 cm^{-1} where HITRAN cross-sections are larger with peaks of $\approx 5 \times 10^{-20}\,\mathrm{cm}^2$, which would be optically thick for abundances $\geq 10^{-7}$.

– NH_3: the HITRAN and PNNL cross-sections agree well.

– O_3: there is no PNNL data for this gas.

– C_2H_2: the HITRAN and PNNL cross-sections agree well.

– HCOOH: The HITRAN data between 1000–1200 and 1725–1875 cm^{-1} agrees with the PNNL data. The PNNL cross-sections indicate missing line data over the range 550–1000 cm^{-1} with peaks of $\approx 5 \times 10^{-19}\,\mathrm{cm}^2$, which would be optically thick for abundances $\geq 10^{-8}$., 1200–1725 cm^{-1}, and 1875–2000 cm^{-1} with peaks of $\approx 5 \times 10^{-20}\,\mathrm{cm}^2$, which would be optically thick for abundances $\geq 10^{-7}$.

– CH_3Cl: The HITRAN and PNNL cross-sections agree well. PNNL cross-sections indicate missing line data around 600 cm^{-1}.

– HCN: the HITRAN and PNNL cross-sections agree well.

– PH_3: the HITRAN and PNNL cross-sections agree well.

– C_2H_4: The HITRAN data is about an order of magnitude less than PNNL. Therefore, the PNNL data suggests the abundances should be an order of magnitude less to obtain the same forcings as the HITRAN data.

– OCS: the HITRAN and PNNL cross-sections agree well.

– HOCl: there is no PNNL data for this gas.

– N_2O: the HITRAN and PNNL cross-sections agree well.

– NO_2: The HITRAN and PNNL cross-sections agree well in the range 1550–1650 cm^{-1}. The PNNL cross-sections are up to an order of magnitude larger than HITRAN for cross-sections in the range 650–850 cm^{-1} and around 1400 cm^{-1}. PNNL cross-sections indicate missing line data over the ranges 850-1100 cm^{-1} and 1650–2000 cm^{-1} with peaks of $\approx 10^{-19}\,\mathrm{cm}^2$, which would be optically thick for abundances $\geq 5 \times 10^{-7}$.

– C_2H_6: the HITRAN and PNNL cross-sections agree well.

– HO_2: there is no PNNL data for this gas.

– ClO: there is no PNNL data for this gas.

– OH: there is no PNNL data for this gas.

– HF: The HITRAN and PNNL data do not overlap. The HITRAN data is available below 500 cm^{-1} and PNNL data is available above $\approx$900 cm^{-1}.

– H_2S: The HITRAN and PNNL cross-sections agree well in the range 1100–1400 cm^{-1}. There is no PNNL data for the absorption feature at wavenumbers less that 400 cm^{-1}.

– H_2CO: The HITRAN and PNNL cross-sections agree well for the absorption band in the range 1600–1850 cm^{-1}. The HITRAN data is missing the absorption band over the wavenumber range 1000–1550 cm^{-1} with peaks of $\approx 10^{-20}\,\mathrm{cm}^2$, which would be optically thick for abundances $\geq 5 \times 10^{-6}$.

– HCl: there are no optically thick absorption features over the wavenumbers where PNNL data exists.

The spectral data described above only covers the thermal spectrum. HITRAN line parameters are not available for the solar spectrum (other than CO_2, CH_4, H_2O, and O_3). We are unaware of any absorption data for these gases in the solar spectrum. If these gases are strong absorbers in the solar spectrum (e.g. O_3) the radiative forcing calculations could be significantly affected. Very strong heating in the stratosphere would cause dramatic differences in the stratospheric structure which would significantly affect the radiative forcing.

2.3 Atmospheric profile

We perform our calculations for a single-column atmosphere. Performing radiative forcing calculations for a single profile rather than multiple profiles representing the meridional variation in the Earth's climatology introduces only small errors (Myhre and Stordal, 1997; Freckleton et al., 1998; Byrne and Goldblatt, 2014).

The tropospheric temperature structure is dictated largely by convection. We approximate the tropospheric temperature structure with the pseudo-adiabatic lapse rate. The lapse

rate is dependent on both pressure and temperature. There is a large range of uncertainty in the surface temperatures of the Archean, we take the surface temperature to be the Global and Annual Mean (GAM) temperature on the modern Earth (289 K). We chose this temperature for two reasons. (1) It makes comparisons with the modern Earth straight forward. (2) Glaciations appear rare in the Archean (Young, 1991), thus, it is expected that surface temperatures were likely as warm as today for much of the Archean. Therefore, modern day surface temperatures are a reasonable assumption for our profile.

We calculate three atmospheric profiles for N_2 inventories of 0.5 bar, 1 bar, and 2 bar. Atmospheric pressure varies with the addition of CO_2 and CH_4. We use the GAM relative humidity from Modern Era Retrospective-analysis for Research and Applications reanalysis data products (Rienecker et al., 2011) over the period 1979 to 2011.

In contrast to the troposphere, the stratosphere (taken to be from the tropopause to the top of the atmosphere) is near radiative equilibrium. The stratospheric temperature structure is therefore sensitive to the abundances of radiatively active gases. For a grey gas, an optically thin stratosphere heated by upwelling radiation will be isothermal at the atmospheric skin temperature ($T = (I(1-\alpha)/8\sigma)^{1/4} \approx 203\,\mathrm{K}$, Pierrehumbert, 2010). We take this to be the case in our calculations. In reality, non-grey gases can give a warmer or cooler stratosphere depending on the spectral positioning of the absorption lines. Furthermore, the stratosphere would not have been optically thin, as CO_2 (and possibly other gases) were likely optically thick for some wavelengths, which would have cooled the stratosphere. Other gases, such as CH_4, may have significantly warmed the stratosphere by absorbing solar radiation. However, the abundances of these gases are poorly constrained. Since there is no convincing reason to choose any particular profile, we keep the stratosphere at the skin temperature for simplicity. The atmospheric profiles are shown in figure 2. We take the tropopause as the atmospheric level at which the pseudoadiabatic lapse rate reaches the skin temperature. Sensitivity tests were performed to examine the sensitivity of radiative forcing to the temperature and water vapour structure. We find that differences in radiative forcing are generally small ($\leq 10\,\%$, appendix A).

In this study, we explicitly include clouds in our radiative transfer calculations. Following Kasting et al. (1984), many RCMs used to study the Archean climate have omitted clouds, and adjusted the surface albedo such that the modern surface temperatures can be achieved with the current atmospheric composition and insolation. Goldblatt and Zahnle (2011b) showed that neglecting the effects of clouds on longwave radiation can lead to significant over-estimates of radiative forcings, as clouds absorb longwave radiation strongly and with weak spectral dependence. Clouds act as a new surface of emission to the top of the atmosphere and, therefore, the impact on the energy budget of molecular absorption between clouds and the surface is greatly reduced. We take our cloud climatology as cloud fractions and optical depths from International Satellite Cloud Climatology Project D2 data set, averaging from January 1990 to December 1992. This period is used by Rossow et al. (2005) and was chosen so that we could compare cloud fractions. We assume random overlap and average by area to estimate cloud fractions. The clouds were placed at 226 K for high clouds, 267 K for middle clouds and 280 K for low clouds, this corresponds to the average temperature levels of clouds on the modern Earth. Cloud properties are taken from Byrne and Goldblatt (2014). The cloud climatology of the Archean atmosphere is highly uncertain. Recent GCM studies have found that there may have been less cloud cover due to less surface heating from reduced insolation (Charnay et al., 2013; Wolf and Toon, 2013). Other studies have suggested other mechanisms which could have caused significant changes in cloud cover during the Archean (Rondanelli and Lindzen, 2010; Rosing et al., 2010; Shaviv, 2003) although theoretical problems have been found with all of these studies (Goldblatt and Zahnle, 2011b, a). Nevertheless, given the large uncertainties in the cloud climatology in the Archean the most straight forward assumption is to assume modern climatology, even though there were likely differences in the cloud climatology. Furthermore, the goal of this study is to examine greenhouse forcings and not cloud forcings. Therefore, we want to capture the longwave effects of clouds to a first order degree. Differences in cloud climatology have only secondary effects on the results given here.

Atmospheric profiles are provided as supplementary material.

2.4 Radiative forcing calculations

We use the Spectral Mapping for Atmospheric Radiative Transfer (SMART) code, written by David Crisp (Meadows and Crisp, 1996), for our radiative transfer calculations. This code works at line-by-line resolution but uses a spectral mapping algorithm to treat different wavenumber regions with similar optical properties together, giving significant savings in computational cost. We evaluate the radiative transfer in the range 50–100,000 cm^{-1} (0.1–200 μm) as a combined solar and thermal calculation.

Radiative forcing is calculated by performing radiative transfer calculations on atmospheric profiles with perturbed and unperturbed greenhouse gas abundances and taking the difference in net flux of radiation at the tropopause. We assume the gases examined here are well-mixed.

3 Results and discussion

3.1 CO_2

We calculate CO_2 radiative forcings up to an abundance of 1 (Fig. 3). At 10^{-2}, consistent with paleosol constraints,

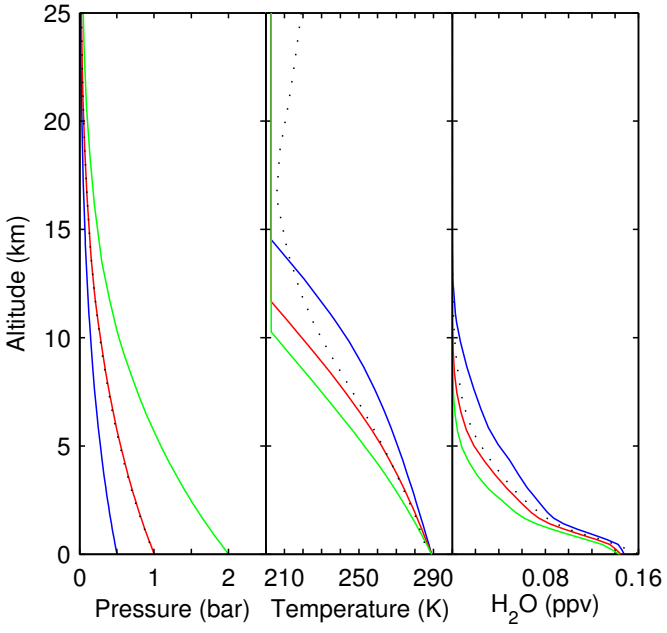

Figure 2. *Atmospheric Profiles.* Pressure, temperature and water vapor structure of atmospheres with 0.5 bar (blue), 1 bar (red), and 2 bar (green) of N_2. The modern atmosphere is also shown (dotted). The water vapor abundances are scaled to an atmosphere with 1 bar of N_2.

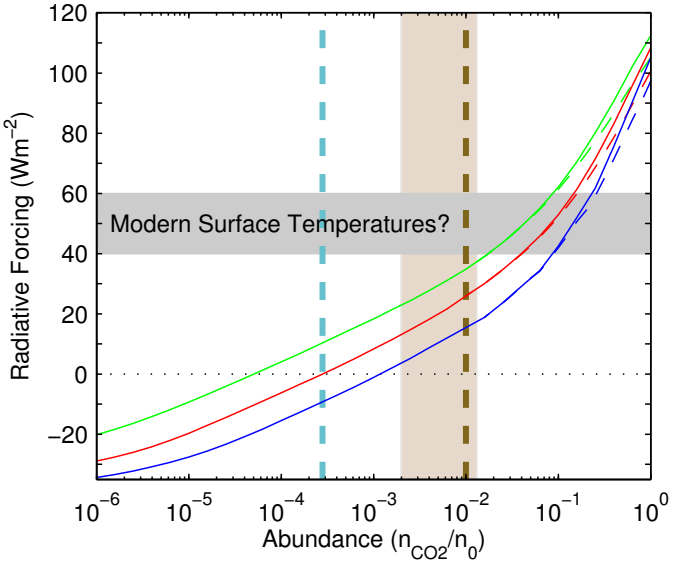

Figure 3. CO_2 *Radiative Forcings.* Radiative forcing as a function of CO_2 abundance, relative to pre-industrial CO_2 (1 bar N_2). Colors are for atmospheres with 0.5 bar, 1 bar, and 2 bar of N_2. Solid lines are calculated with CIA and dashed lines are calculated without CIA. The shaded region shows the range of CO_2 for the early Earth (0.003-0.02 bar, Driese et al., 2011). The vertical dashed blue and brown lines give the pre-industrial and early Earth best guess (10^{-2}) abundances of CO_2.

the radiative forcings are 35 $\mathrm{W\,m^{-2}}$ (2 bar $\mathrm{N_2}$), 26 $\mathrm{W\,m^{-2}}$ (1 bar $\mathrm{N_2}$), and 15 $\mathrm{W\,m^{-2}}$ (0.5 bar $\mathrm{N_2}$), which is considerably short of the forcing required to solve the FYSP, consistent with previous work. The $\mathrm{CO_2}$ forcings given here account for changes in the atmospheric structure due to changes in the $\mathrm{N_2}$ inventory and thus are non-zero at pre-industrial $\mathrm{CO_2}$ for 0.5 bar and 2 bar of $\mathrm{N_2}$. This results in forcings of about 10 $\mathrm{W\,m^{-2}}$ (2 bar) and -9 $\mathrm{W\,m^{-2}}$ (0.5 bar) at pre-industrial $\mathrm{CO_2}$ abundances (see Goldblatt et al., 2009, for a detailed physical description).

At very high $\mathrm{CO_2}$ abundances (> 0.1), $\mathrm{CO_2}$ becomes a significant fraction of the atmosphere. This complicates radiative forcing calculations by (1) changing the atmospheric structure, (2) shortwave absorption/scattering, and (3) uncertainties in the parametrization of continuum absorption. These need careful consideration in studies of very high atmospheric $\mathrm{CO_2}$, so we describe these factors in detail:

1. Large increases in $\mathrm{CO_2}$ increase the atmospheric pressure, and therefore, also increase the atmospheric lapse rate. This results in a cooling of the stratosphere and reduction to the emission temperature. Increased atmospheric pressure also results in the broadening of absorption lines for all of the radiatively active gases. Emissions from colder, higher pressure, layers increases radiative forcing.

2. Shortwave radiation is also affected by very high $\mathrm{CO_2}$ abundances. The shortwave forcing is -2 $\mathrm{W\,m^{-2}}$ at 0.01, -4 $\mathrm{W\,m^{-2}}$ at 0.1 and -18 $\mathrm{W\,m^{-2}}$ at 1. There are two separate reasons for this. The smaller affect is absorption of shortwave radiation by $\mathrm{CO_2}$ which primarily affects wavenumbers less than $\approx 10{,}000\,\mathrm{cm^{-1}}$ (Fig. 4). The most important effect ($\mathrm{CO_2} > 0.1$) is increased Rayleigh scattering due to the increase in the size of the atmosphere. This primarily affects wavenumbers larger than $\approx 10{,}000\,\mathrm{cm^{-1}}$ and is the primary reason for the large difference in insolations through the tropopause for abundances between 0.1 and 1 of $\mathrm{CO_2}$.

3. There is significant uncertainty in the $\mathrm{CO_2}$ spectra at very high abundances. This is primarily due to absorption that varies smoothly with wavenumber that cannot be accounted for by nearby absorption lines. This absorption is termed continuum absorption and is caused by the far wings of strong lines and collision induced absorption (CIA) (Halevy et al., 2009). Halevy et al. (2009) show that different parametrizations of line and continuum absorption in different radiative transfer models can lead to large differences in outgoing longwave radiation at high $\mathrm{CO_2}$ abundances. SMART treats the continuum by using a χ-factor to reduce the opacity of the Voight line shape out to $1000\,\mathrm{cm^{-1}}$ from the line center to match the background absorption. We add to this CIA absorption which has been updated with recent results of Wordsworth et al. (2010). We believe that our radiative transfer runs are as accurate as possible given the poor understanding of continuum absorption.

It is worthwhile comparing our calculated radiative forcings with previous results. In most studies, the greenhouse warming from a perturbation in greenhouse gas abundance is quantified as a change of the GAM surface temperature. We convert our radiative forcings to surface temperatures for comparison. This is achieved using climate sensitivity. Assuming the climate sensitivity to be in the range 1.5–4.5 $\mathrm{W\,m^{-2}}$ (medium confidence range, IPCC, 2013) for a doubling of atmospheric $\mathrm{CO_2}$ and the radiative forcing for a doubling of $\mathrm{CO_2}$ to be 3.7 $\mathrm{Wm^{-2}}$, we find a range of climate sensitivity parameters of 0.4–1.2 $\mathrm{K/Wm^{-2}}$ with a best guess of 0.8 $\mathrm{K/Wm^{-2}}$. We take the $\mathrm{CO_2}$ abundance which gives energy balance at the tropopause (0.20 bar, abundance of 0.13) to be the abundance that gives a surface temperature of 289 K.

The calculated temperature curves are plotted with the results of previous studies (Fig. 5). For all of the studies, surface temperatures were calculated for $0.8\mathrm{S_0}$. However there were differences in the atmospheric pressure: von Paris et al. (2008) and Kienert et al. (2012) have 0.77 bar and 0.8 bar of $\mathrm{N_2}$ respectively, while Haqq-Misra et al. (2008), Wolf and Toon (2013) and Charnay et al. (2013) hold the surface pressure at 1 bar, and remove $\mathrm{N_2}$ to add $\mathrm{CO_2}$.

Model climate sensitivities can be grouped by the type of climate model used. Simple 1-D RCMs (Haqq-Misra et al., 2008; von Paris et al., 2008) have the lowest climate sensitivities (1-4 K). The 3-D models had higher climate sensitivities, but the sensitivities were also more variable between models. Kienert et al. (2012) use a model with a fully dynamic ocean but a statistical dynamical atmosphere. The sea-ice albedo feedback makes the climate highly sensitive to $\mathrm{CO_2}$ abundance and has the largest climate sensitivity (≈18.5 K). Charnay et al. (2013) and Wolf and Toon (2013) use models with fully dynamic atmosphere but with simpler oceans. They generally have climate sensitivities between 2.5-4.5 K but Wolf and Toon (2013) find higher climate sensitivities (7-11 K) for $\mathrm{CO_2}$ concentrations of 10,000–30,000 ppmv due to changes in surface albedo (sea ice extent). The climate sensitivities are larger for the 3-D models compared to the RCMs primarily because of the ice-albedo feedback. Variations in climate sensitivity parameters mask variations in radiative forcings.

The amount of $\mathrm{CO_2}$ required to reach modern day surface temperatures is variable between models. Charnay et al. (2013) and Wolf and Toon (2013) require the least $\mathrm{CO_2}$ to sustain modern surface temperatures (0.06–0.07 bar, abundance of 0.04–0.46), primarily because there are less clouds (low and high), the net effect of which is a decrease in albedo. The cloud feedback in these models works as follows: the reduced insolation results in less surface heating, which results in less evaporation and less cloud formation. The RCM studies require $\mathrm{CO_2}$ abundance very close to our results (0.1-

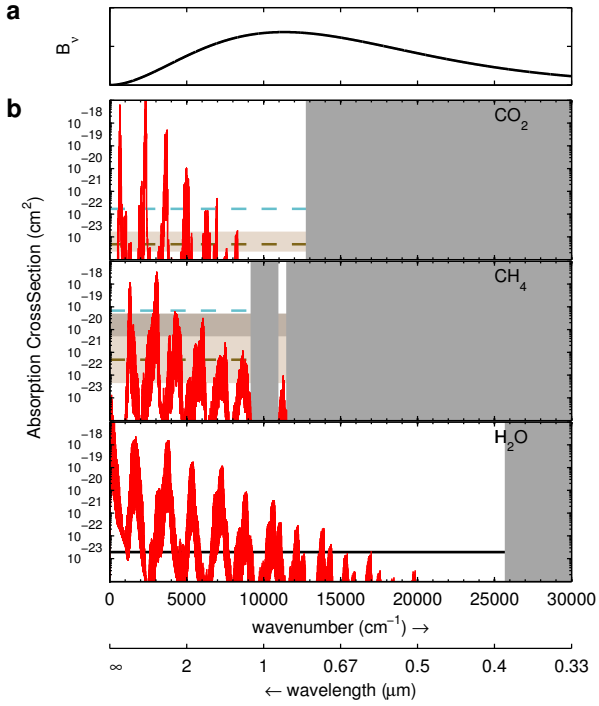

Figure 4. *Solar absorption cross-sections.* (a) Emission spectrum for an object of 5777 K (Effective emitting temperature of modern Sun). (b) Absorption cross-sections of CO_2, CH_4 and H_2O calculated from line data. Grey shading shows were there is no HITRAN line data. Shaded and dashed lines show absorption cross-sections of unity optical depth for abundances given in figures 3 and 6. Solid black line shows the absorption cross-sections of unity optical depth for H_2O.

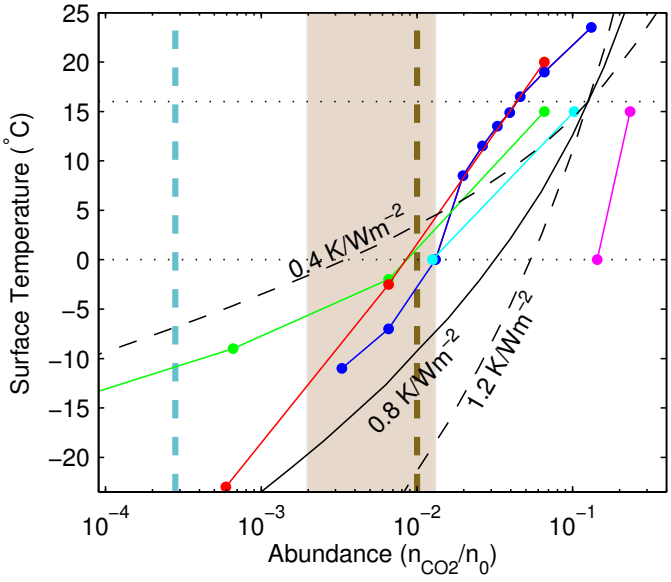

Figure 5. *Surface temperature as a function of* CO_2 *abundance for* $0.8\,S_0$. Temperatures are calculated from radiative forcings assuming climate sensitivity parameters of 0.4 $\mathrm{K/Wm^{-2}}$ (dashed black), 0.8 $\mathrm{K/Wm^{-2}}$ (solid black) and 1.2 $\mathrm{K/Wm^{-2}}$ (dashed black) and a surface temperature of 289 K at 0.20 bar of CO_2 (when our model is in energy balance). The results of Wolf and Toon (2013) (blue), Haqq-Misra et al. (2008) (green), Charnay et al. (2013) (red), von Paris et al. (2008) (cyan), and Kienert et al. (2012) (magenta) are also shown.

0.2 bar, abundance of 0.066–0.13), especially considering differences in atmospheric pressure. Kienert et al. (2012) requires very high CO_2 abundances (≈0.4 bar, abundance of 0.26) to prevent runaway glaciation because of the high sensitivity of the ice-albedo feedback in this model.

3.2 CH_4

We calculate CH_4 radiative forcings up to 10^{-2} (Fig. 6). At abundances greater than 10^{-4} we find considerable shortwave absorption. For an atmosphere with 1 bar of N_2, the shortwave radiative forcing is $\approx 1.4\,\mathrm{Wm^{-2}}$ at 10^{-4}, $\approx 6.7\,\mathrm{Wm^{-2}}$ at 10^{-3}, and $\approx 20\,\mathrm{Wm^{-2}}$ at 10^{-2}. This absorption occurs primarily at wavenumbers less than 11,502 $\mathrm{cm^{-1}}$ where HITRAN data is available (Fig. 4). We find much more shortwave absorption here than in studies from Jim Kasting's group (Pavlov et al., 2000; Haqq-Misra et al., 2008) which also parametrize solar absorption. The reason for this discrepancy is likely due to improvements in the spectroscopic data. We repeated our radiative forcing calculations using HITRAN 2000 line parameters and found only minor differences in the longwave absorption but much less absorption at solar wavelengths (Fig. 7). Figure 8 shows the solar absorption by CH_4 using spectra from the 2000 and 2012 editions of HITRAN. There is a significant increase in shortwave absorption between 5500–9000 $\mathrm{cm^{-1}}$ and around 11,000 $\mathrm{cm^{-1}}$.

Very strong shortwave absorption would have a significant effect on the temperature structure of the stratosphere. Strong absorption would lead to strong stratospheric warming which would limit the usefulness of our results. Nevertheless, our calculations indicate that at 10^{-4} of CH_4 the combined thermal and solar radiative forcings are 7.6 $\mathrm{W\,m^{-2}}$ (2 bar of N_2), 7.2 $\mathrm{W\,m^{-2}}$ (1 bar of N_2), and 6.2 $\mathrm{W\,m^{-2}}$ (0.5 bar of N_2) and the thermal radiative forcings are 9.8 $\mathrm{W\,m^{-2}}$ (2 bar of N_2), 8.6 $\mathrm{W\,m^{-2}}$ (1 bar of N_2), and 6.8 $\mathrm{W\,m^{-2}}$ (0.5 bar of N_2). Therefore, excluding the effects of overlap (which are minimal, Byrne and Goldblatt, 2014), the combined thermal and solar radiative forcing due to 10^{-3} of CO_2 and 10^{-4} of CH_4 are 42.6 $\mathrm{W\,m^{-2}}$ (2 bar of N_2), 33.2 $\mathrm{W\,m^{-2}}$ (1 bar of N_2) and 21.2 $\mathrm{W\,m^{-2}}$ (0.5 bar of N_2), significantly short of the forcings needed to sustain modern surface temperatures. It should be noted that strong solar absorption makes the precise radiative forcing highly sensitive to the position of the tropopause because this is the altitude at which most of the shortwave absorption is occurring. Therefore, small changes in the position of the tropopause result in large changes in the shortwave forcing. The surface temperature response to this forcing is less straight forward and the linearity between forcing and surface temperature change may breakdown Hansen et al. (2005).

These calculations do not consider the products of atmospheric chemistry. Numerous studies have found that high CH_4:CO_2 ratios lead to the formation of organic haze in low O_2 atmospheres which exerts an anti-greenhouse effect (Kasting et al. , 1983; Zahnle, 1986; Pavlov et al., 2000; Haqq-Misra et al., 2008). Organic haze has been predicted by photochemical modelling at CH_4:CO_2 ratios larger than 1 (Zahnle, 1986), and laboratory experiments have found that organic haze could form at CH_4:CO_2 ratios as low as 0.2–0.3 (Trainer et al., 2004, 2006).

As with CO_2, we compare our CH_4 radiative forcings to values given in literature (Fig. 9). Temperatures are calculated from radiative forcings assuming a surface temperature of 271 K for an abundance of 0 and climate sensitivity parameters of 0.4 $\mathrm{K/Wm^{-2}}$, 0.8 $\mathrm{K/Wm^{-2}}$ and 1.2 $\mathrm{K/Wm^{-2}}$, and a background CO_2 abundance of 10^{-2}. Due to absorption of shortwave radiation, our calculated surface temperatures decrease for abundances above 10^{-3}. Assuming a linear relationship between forcing and climate response is likely a poor assumption given strong atmospheric solar absorption. Results from Pavlov et al. (2000) are included even though they are known to be erroneous as an illustration of the utility of these comparisons. All other studies give similar surface temperatures. However, these studies lack the strong solar absorption from the HITRAN 2012 database. Haqq-Misra et al. (2008) shortwave radiative transfer is parametrized from data which pre-dates HITRAN 2000 and Wolf and Toon (2013) only include CH_4 absorption below 4650 $\mathrm{cm^{-1}}$ where changes to the spectra are not significant.

3.3 Trace gases

The chemical cycles of several other greenhouse gases have been studied in the Archean. It has been hypothesized that higher atmospheric abundances could have been sustained making these gases important for the planetary energy budget. High abundances of NH_3 (Sagan and Mullen, 1972), C_2H_6 (Haqq-Misra et al., 2008), N_2O (Buick, 2007), and OCS (Ueno et al., 2009) have all been proposed in the Archean. There are many other greenhouse gases in the HITRAN database that have not been studied, whether these gases could have been sustained at radiatively important abundances is beyond the scope of this paper. We review the sources, concentrations, and lifetimes from the strongest gases in table 1 (modern Earth). We also provide a review of the relevant literature on these gases in the Archean. Here we quantify the warming these gases could have provided in the Archean, motivated by future proposals of these as warming agents.

3.3.1 Radiative forcings

We produce a first order estimate of the relative absorption strength of the HITRAN gases by taking the product of the irradiance produced by a blackbody of 289 K and the absorption cross-sections to get the absorption per molecule of a gas when saturated with radiation (Fig. 10). Using this metric, H_2O ranks as the 11^{th} strongest greenhouse gas, and CO_2 and CH_4 rank 16^{th} and 27^{th} respectively. This demonstrates

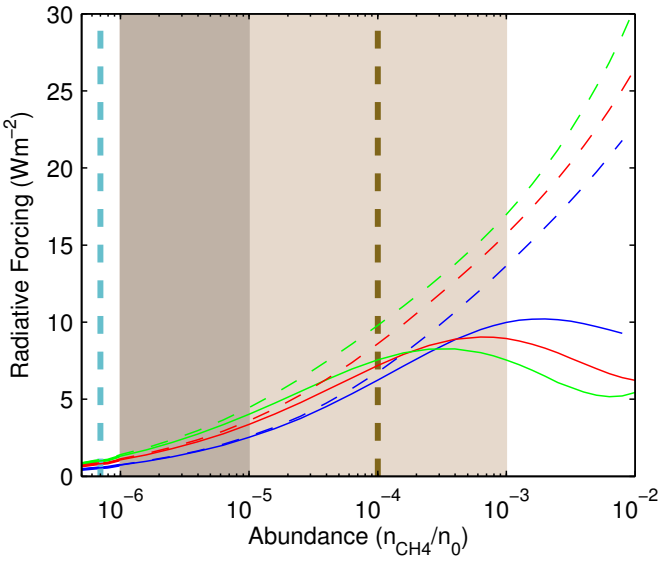

Figure 6. Radiative Forcing for CH_4. Radiative forcing as a function of CH_4 for atmospheres with 0.5 bar (blue), 1 bar (red) and 2 bar (green) of N_2. Dashed curves show the longwave forcing. Shaded region shows the range of CH_4 for the early Earth that could be sustained by abiotic (dark) and biotic (light) sources (Kasting, 2005). The vertical dashed blue and brown lines give the pre-industrial and early Earth best guess (100 ppmv, Goldblatt et al., 2006) abundances of CH_4.

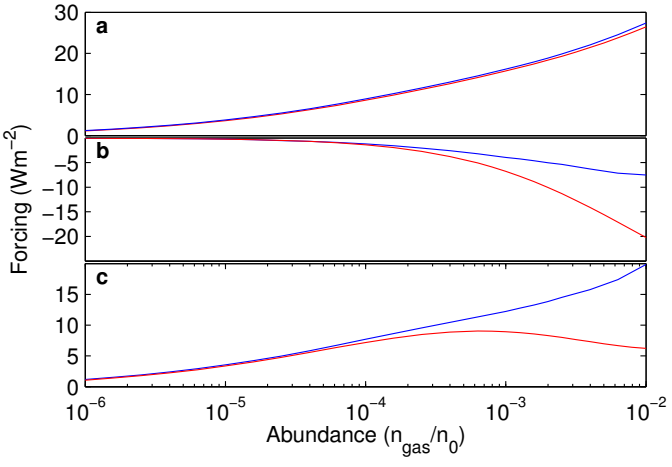

Figure 7. CH_4 *forcings using HITRAN 2000 and 2012 spectral data.* **(a)** Longwave, **(b)** Shortwave, and **(c)** combined longwave and shortwave radiative forcings using HITRAN 2000 (blue) and 2012 (red) spectral data.

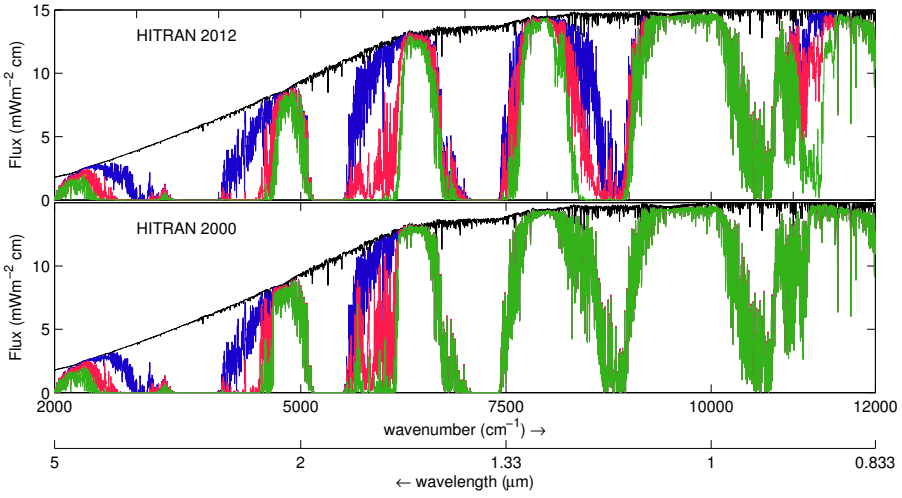

Figure 8. *Downward shortwave flux.* Insolation at the top of the atmosphere (black) and surface for CH_4 abundances 10^{-6} (blue), 10^{-4} (red), and 10^{-2} (green) using HITRAN 2012 (top) and HITRAN 2000 (bottom) line data.

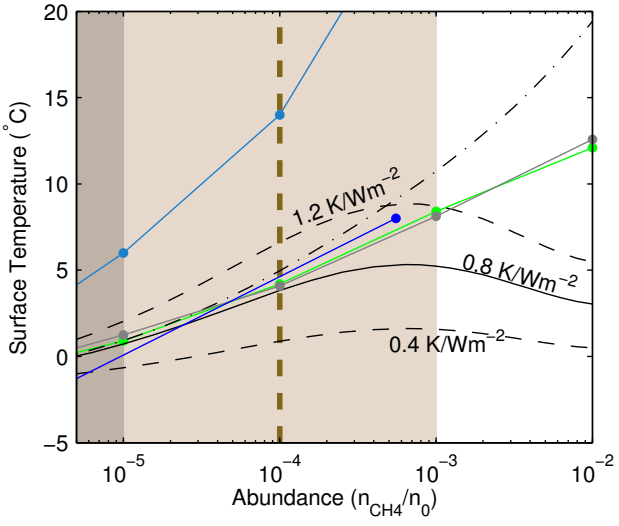

Figure 9. *Surface temperature as a function of* CH_4 *abundance for* $0.8\,S_0$. Temperatures are calculated from radiative forcings assuming a surface temperature of 271 K for 0 ppmv of CH_4 and climate sensitivity parameters of 0.4 K/Wm^{-2} (dashed black), 0.8 K/Wm^{-2} (solid black) and 1.2 K/Wm^{-2} (dashed black) and a background CO_2 abundance of 10^{-2}. Dashed-Dotted black line shows the longwave radiative forcing. The results of Wolf and Toon (2013) (blue), Haqq-Misra et al. (2008) (green), Pavlov et al. (2000) (turquoise), and Kiehl and Dickinson (1987) (grey) are also plotted. Temperatures for Kiehl and Dickinson (1987) are found from radiative forcings assuming a climate sensitivity parameter of 0.81 K/Wm^{-2} and a surface temperature of 271 K for 0 ppmv of CH_4.

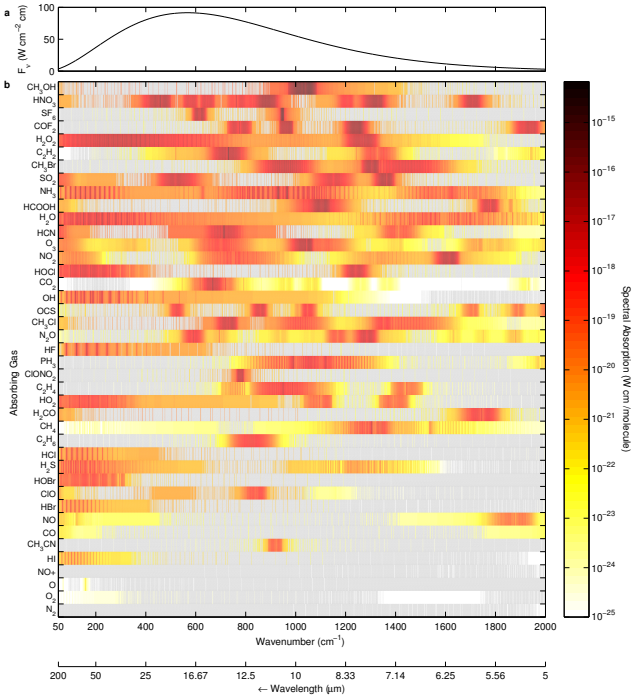

Figure 10. *Spectral absorption of blackbody emissions.* **(a)** Emission intensity from a blackbody of 289 K. **(b)** Product of emission intensity and absorption cross-sections for gases from the HITRAN 2012 database. Gases are ordered by decreasing spectrum integrated absorption strength from top to bottom. Grey indicates wavenumbers where no absorption data is available. Absorption coefficients were calculated at 500 hPa and 260 K.

that many of the HITRAN gases are strong greenhouse gases and that it is conceivable that low abundances of these gases could have a significant effect on the energy budget.

We calculate the radiative forcings for the HITRAN gases which produce forcings greater than 1 $\mathrm{W\,m^{-2}}$ over the abundances of 10^{-8} to 10^{-5} (Fig. 11), assuming the gases are well-mixed. The radiative forcings are calculated in an atmosphere which contains only H_2O and N_2. Many of the gases reach forcings greater than 10 $\mathrm{Wm^{-2}}$ at abundances less than 10^{-6}.

We give rough estimates of the expected radiative forcings assuming the PNNL cross-sections are correct for gases for which the HITRAN and PNNL cross-sections disagree. We have made approximate corrections to the forcings as follows. For some gases the shape of the absorption cross-sections were the same but the magnitude was offset. For these gases, we adjust the abundances required for a given forcing, this was done for CH_3OH (x10), CH_3Br (x13), C_2H_4 (x0.1), and H_2O_2 (x2). Missing spectra was compensated for by adding the radiative forcings from other gases that had similar spectra. For CH_3OH the C_2H_4 forcings were added. For HCOOH we added the HCN forcing. For NO_2 we added the HOCl forcing. For H_2CO we added the PH_3 forcing for a given abundance scaled up an order of magnitude.

There are significant differences in radiative forcing due to different N_2 inventories. The differences in radiative forcing due to differences in atmospheric pressure varies from gas to gas. Generally, the differences in forcing due to differences in atmospheric structure are similar, but the differences due to pressure broadening are more variable. Broadening is most effective for gases which have broad absorption features with highly variable cross-sections because the broadening of the lines covers areas with weak absorption. Such gases include NH_3, HCN, C_2H_2 and PH_3. At 5×10^{-6}, 55-60 percent of the difference in radiative forcing between atmospheres can be attributed to pressure broadening for these gases. Where as, NO_2 and HOCl which have strong but narrow absorption features show the least difference in forcing due to pressure broadening (20-23 %).

3.3.2 Overlap

Here we examine the reduction in radiative forcing due to overlap for gases which reach radiative forcings of 10 $\mathrm{W\,m^{-2}}$ at abundances less than 10^{-5}. The abundances of CO_2 and CH_4 are expected to be quite high in the Archean. Trace gases which have absorption bands coincident with the

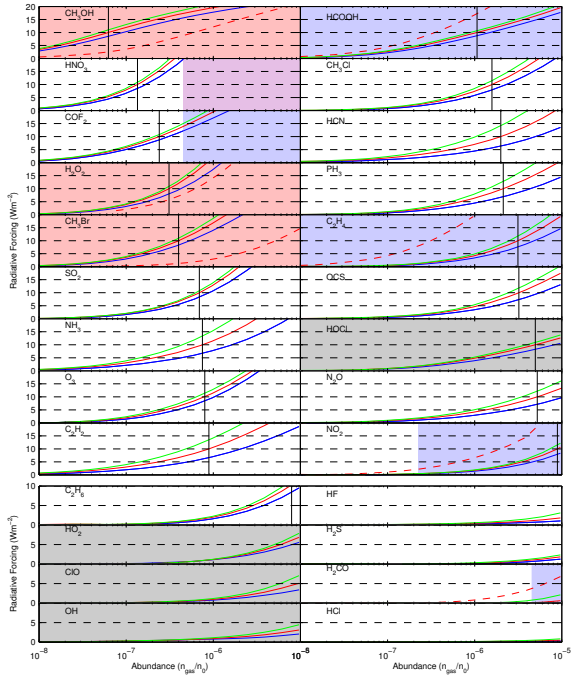

Figure 11. *Trace gas radiative forcings.* All sky radiative forcings for potential early Earth trace gases, colors are as in Fig. 2. Gases are ordered by the concentration required to get a radiative forcing of $10\,\mathrm{W\,m^{-2}}$. Shading indicates concentrations where computed cross-sections from HITRAN data were in poor agreement with the PNNL data. The colors indicate areas where HITRAN data underestimates (blue), overestimates (red), or both at different frequencies (purple). Grey shading indicates where no PNNL data was available. Vertical black lines show the concentration at which the radiative forcing is $10\,\mathrm{W\,m^{-2}}$ for a 1 bar atmosphere. Dotted red lines give rough estimates of the radiative forcing accounting for incorrect spectral data. Concentrations are scaled to an atmosphere with 1 bar of N_2.

absorption bands of CO_2 and CH_4 will be much less effective at warming the Archean atmosphere.

We examine the effect of overlap on radiative forcing by looking at several cases with varying abundances of CO_2, CH_4 (Fig. 12), and other trace gases (Fig. 13). The magnitude of overlap can vary substantially between the gases in question. For the majority of gases overlap with CO_2 is the largest. The reduction in forcing is generally between 10–30 % but can be as high as 86 %. The reduction in forcing are largest for HCN (86 %), C_2H_2 (78 %), CH_3Cl (71 %), NO_2 (52 %), and N_2O (33 %) all with 10^{-2} of CO_2. All of these gases have significant absorption bands in the 550-850 $\mathrm{cm^{-1}}$ wavenumber region where CO_2 absorbs the strongest. Of particular interest is N_2O which has previously been proposed to have built up to significant abundances on the early Earth (Buick, 2007). C_2H_2 could also have been produced by a hypothetical early Earth haze, although previous studies have found that it would not build up to radiatively important abundances (Haqq-Misra et al., 2008).

The reduction in forcing due to CH_4 is generally less than 20 % but can be as high as 37 %. The reductions in forcing are largest for HOCl (33 %), N_2O (32 %), COF_2 (25 %), and H_2O_2 (21 %) all with 10^{-4} of CH_4. All of which have absorption bands in 1200–1350 $\mathrm{cm^{-1}}$. As with CO_2, the radiative forcing from N_2O is significantly reduced due to overlap with CH_4, suggesting that N_2O is not a good candidate to produce significant warming on early Earth except at very high abundances.

We calculate the reduction in radiative forcing due to overlap between trace gases (Fig. 13). There is a large amount of overlap between C_2H_2, CH_3Cl and HCN resulting in a reduction in radiative forcing of $\approx 30\,\%$. All three gases have their strongest absorption bands in the region 700–850 $\mathrm{cm^{-1}}$ and have a secondary absorption band in the region 1250–1500 $\mathrm{cm^{-1}}$ which are on the edges of the water vapour window. All three gases have significant overlap with CO_2, for an atmosphere with 10^{-2} of CO_2 the reductions in forcing are $> 70\,\%$.

Other traces gases with significant overlap are COF_2 and HOCl (37 %) due to coincident absorption bands at $\approx 1250\mathrm{cm^{-1}}$, and CH_3OH and PH_3 (30 %) due to coincident absorption around $\approx 1000\mathrm{cm^{-1}}$.

Other background absorption could have been present which would have had overlapping absorption with these gases. Wordsworth and Pierrehumbert (2013) have proposed that elevated N_2 and H_2 levels may have been present in the Archean which would have resulted in significant N_2–H_2 CIA across much of the infrared spectrum including the water vapour window. Overlap between N_2–H_2 absorption and the gases examined here would likely be significant as

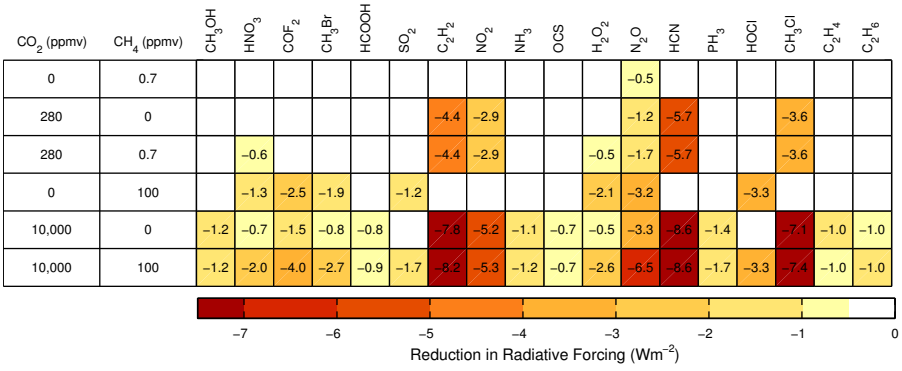

Figure 12. *Overlap with* CO_2 *and* CH_4. Reduction in radiative forcing due to overlapping absorption. Trace gas concentrations are held at the concentrations which gives a $10\,\mathrm{W\,m^{-2}}$ radiative forcing for an atmosphere with $1\,\mathrm{bar}$ of N_2.

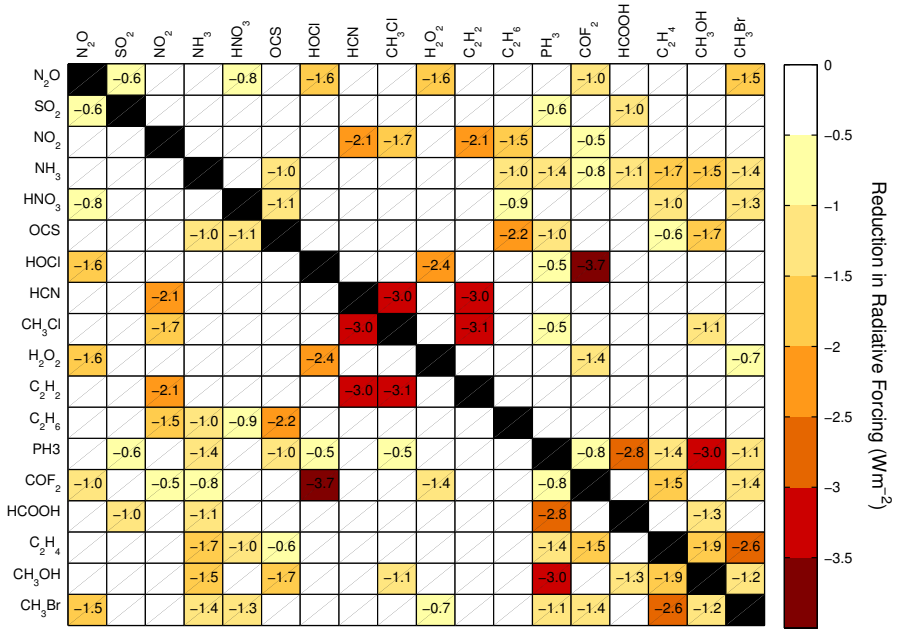

Figure 13. *Trace gas overlap.* Reduction in radiative forcing due to overlapping absorption. Gas concentrations are held at concentrations which give a $10\,\mathrm{W\,m^{-2}}$ radiative forcing for an atmosphere with $1\,\mathrm{bar}$ of N_2.

many of these gases have significant absorption in the water vapour window. However, performing these overlap calculations is beyond the scope of this work.

3.3.3 Comparison between our results and previous calculations

We compare inferred radiative forcings from prior work to ours using the same method as for CO_2 and CH_4 (Fig. 14).

Inferred C_2H_6 radiative forcings from Haqq-Misra et al. (2008) for a 1 bar atmosphere agree well with our results. Inferred NH_3 from Kuhn and Atreya (1979) for a 0.78 bar atmosphere agree well with our results, although, our results suggest that the results of Kuhn and Atreya (1979) are on the lower end of possible temperature changes. Inferred N_2O from Roberson et al. (2011) for a 1 bar atmosphere agree well with our results. Roberson et al. (2011) perform radiative forcing calculations with CO_2 and CH_4 abundances of 320 ppmv and 1.6 ppmv. Due to overlap this forcing is likely reduced by ≈50 % with early Earth CO_2 and CH_4 abundances of 10^{-2} and 10^{-4}. Ueno et al. (2009) give a rough estimate of the radiative forcing due to 10 ppmv of OCS to be 60 $\mathrm{W\,m^{-2}}$. In this work we find the forcing to be much less than this (≈ 20 $\mathrm{Wm^{-2}}$).

4 Conclusions

Using the SMART radiative transfer model and HITRAN line data, we have calculated radiative forcings for CO_2, CH_4 and 26 other HITRAN greenhouse gases on a hypothetical early Earth atmosphere. These forcings are available at several background pressures and we account for overlap between gases. We recommend the forcings provided here be used both as a first reference for which gases are likely good greenhouse gases, and as a standard set of calculations for validation of radiative forcing calculations for the Archean. Model output are available as supplementary material for this purpose. Many of these gases can produce significant radiative forcings at low abundances. Whether any of these gases could have been sustained at radiatively important abundances during the Archean requires study with geochemical and atmospheric chemistry models.

Comparing our calculated forcings with previous work, we find that CO_2 radiative forcings are consistent, but find a stronger shortwave absorption by CH_4 than previously recorded. This is primarily due to updates to the HITRAN databse at wavenumbers less than 11,502 $\mathrm{cm^{-1}}$. This new result suggests an upper limit to the warming CH_4 could have provided of about 10 $\mathrm{W\,m^{-2}}$ at 5×10^{-4}–10^{-3}. Amongst the trace gases, we find that the forcing from N_2O was likely overestimated Roberson et al. (2011) due to underestimated overlap with CO_2 and CH_4, and that the radiative forcing from OCS was greatly overestimated by Ueno et al. (2009).

Appendix A: Sensitivity

Figure A1 shows the fluxes, radiative forcings and percentage difference in radiative forcings for various possible GAM temperature and water vapour profiles for the early Earth. The effect on radiative forcing calculations from varying the stratospheric temperature from 170 to 210 K while the tropopause temperature is kept constant are very small ($<$ 3 %). Varying the tropopause temperature between 170 and 210 K results in larger differences in radiative forcing ($<$ 10 %). Changing the relative humidity effects radiative forcing by less than 5 %. Radiative forcing calculations are sensitive to surface temperature. Increasing or decreasing a 290 K surface temperature by 10 K results in differences in radiative forcing of $\leq$ 12 %. However, the difference in forcing between 270 and 290 K is much larger (12–25 %).

The Supplement related to this article is available online at doi:10.5194/cp-0-1-2014-supplement.

Acknowledgements. We thank Ty Robinson for help with SMART and discussions of the theory behind it. Financial support was received from the Natural Sciences and Engineering Research Council of Canada (NSERC) CREATE Training Program in Interdisciplinary Climate Science at the University of Victoria (UVic); a University of Victoria graduate fellowship to B.B. and NSERC Discovery grant to C.G. This research has been enabled by the use of computing resources provided by WestGrid and Compute/Calcul Canada. We would also like to thank Andrew MacDougall for helpful comments on an earlier draft of the manuscript and Kevin Zahnle for sharing is insights and reviewing the information in table 1. We thank Jim Kasting and an anonymous reviewer for comments which improved the manuscript.

References

Abad, G. G., Allen, N. D. C., Bernath, P. F., Boone, C. D., McLeod, S. D., Manney, G. L., Toon, G. C., Carouge, C., Wang, Y., Wu, S., Barkley, M. P., Palmer, P. I., Xiao, Y., and Fu, T. M.: Ethane, ethyne and carbon monoxide abundances in the upper troposphere and lower stratosphere from ACE and GEOS-Chem: a comparison study, Atmos. Chem. Phys., 11, 9927–9941, doi:10.5194/acp-11-9927-2011, 2011.

Allen, N. D. C., Abad, G. G., Bernath, P. F., and Boone, C. D.: Satellite observations of the global distribution of hydrogen peroxide (H2O2) from ACE, J. Quant. Spectrosc. Radiat. Transfer, 115, 66-77, doi:10.1016/j.jqsrt.2012.09.008, 2013.

Bar-Nun, A. and Chang, S.: Photochemical reactions of water and carbon-monoxide in Earth's primitive atmosphere, J. Geophys. Res.-Oc. Atm., 88, 6662–6672, doi:10.1029/JC088iC11p06662, 1983.

Buick, R.: Did the Proterozoic "Canfield Ocean" cause a laughing gas greenhouse?, Geobiology, 5, 97–100, doi:10.1111/j.1472-4669.2007.00110.x, 2007.

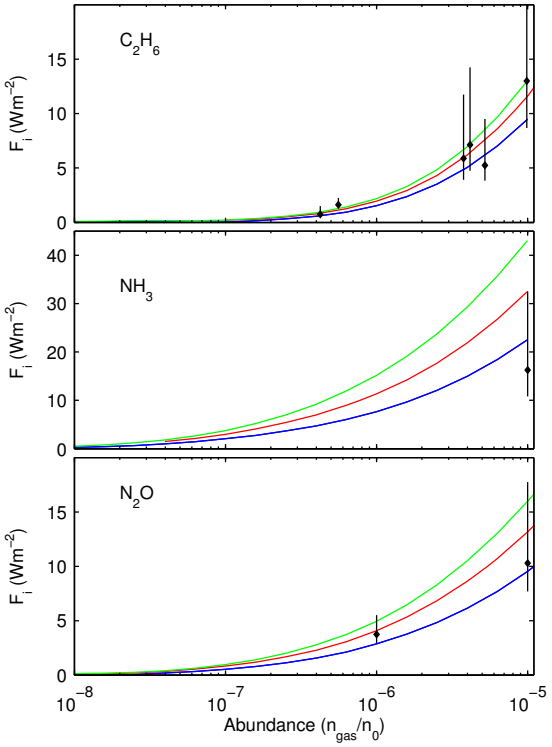

Figure 14. *Calculated Radiative forcings and inferred radiative forcings from literature.* Literature radiative forcings are inferred from temperature changes reported by Haqq-Misra et al. (2008) (C_2H_6), Kuhn and Atreya (1979) (NH_3) and Roberson et al. (2011) (N_2O). Radiative forcings are calculated assuming a range of climate sensitivity parameters of 0.4 to 1.2 $K(Wm^{-2})^{-1}$ with a best guess of 0.8 $K(Wm^{-2})^{-1}$.

Byrne, B. and Goldblatt, C.: Radiative forcing at high concentrations of well-mixed greenhouse gases, Geophys. Res. Lett., 41, 152–160, doi:10.1002/2013GL058456, 2014.

Charnay, B., Forget, F., Wordsworth, R., Leconte, J., Millour, E., Codron, F., and Spiga, A.: Exploring the faint young Sun problem and the possible climates of the Archean Earth with a 3-D GCM, J. Geophys. Res.-Atmos., 118, 10414, doi:10.1002/jgrd.50808, 2013.

Chebbi, A. and Carlier, P.: Carboxylic acids in the troposphere, occurrence, sources, and sinks: a review, Atmos. Environ., 30, 4233–4249, doi:10.1016/1352-2310(96)00102-1, 1996.

Chin, M. and Davis, D.: A reanalysis of carbonyl sulfide as a source of stratospheric background sulfur aerosol, J. Geophys. Res.-Atmos., 100, 8993–9005, doi:10.1029/95JD00275, 1995.

Domagal-Goldman, S. D., Meadows, V. S., Claire, M. W., and Kasting, J. F.: Using biogenic sulfur gases as remotely detectable biosignatures on anoxic planets, Astrobiology, 11, 419–441, doi:10.1089/ast.2010.0509, 2011.

Donn, W. L., Donn, B. D., and Valentine, W. G.: On the early history of the Earth, Geol. Soc. Am. Bull., 76, 287–306, doi:10.1130/0016-7606(1965)76[287:OTEHOT]2.0.CO;2, 1965.

Driese, S. G., Jirsa, M. A., Ren, M., Brantley, S. L., Sheldon, N. D., Parker, D., and Schmitz, M.: Neoarchean paleoweathering of tonalite and metabasalt: implications for reconstructions of 2.69 Gyr early terrestrial ecosystems and paleoatmospheric chemistry, Precambrian Res., 189, 1–17, doi:10.1016/j.precamres.2011.04.003, 2011.

Duchatelet, P., Mahieu, E., Ruhnke, R., Feng, W., Chipperfield, M., Demoulin, P., Bernath, P., Boone, C. D., Walker, K. A., Servais, C., and Flock, O.: An approach to retrieve information on the carbonyl fluoride (COF_2) vertical distributions above Jungfraujoch by FTIR multi-spectrum multi-window fitting, Atmos. Chem. Phys., 9, 9027–9042, 2009.

Feulner, G.: The faint young sun problem, Rev. Geophys., 50, RG2006, doi:10.1029/2011RG000375, 2012.

Fishman, J. and Crutzen, P.: Origin of ozone in the troposphere, Nature, 274, 855–858, doi:10.1038/274855a0, 1978.

Freckleton, R., Highwood, E., Shine, K., Wild, O., Law, K., and Sanderson, M.: Greenhouse gas radiative forcing: Effects of averaging and inhomogeneities in trace gas distribution, Q. J. Roy. Meteorol. Soc., 124, 2099–2127, doi:10.1256/smsqj.55013, 1998.

Gaillard, F., Scaillet, B., and Arndt, N. T.: Atmospheric oxygenation caused by a change in volcanic degassing pressure, Nature, 478, 229–U112, doi:10.1038/Nature10460, 2011.

Glindemann, D., Edwards, M., and Kuschk, P.: Phosphine gas in the upper troposphere, Atmos. Environ., 37,2429–2433, doi:10.1016/S1352-2310(03)00202-4, 2003.

Glindemann, D., Edwards, M., and Schrems, O.: Phosphine and methylphosphine production by simulated lightning - a study for the volatile phosphorus cycle and cloud forma-

tion in the earth atmosphere, Atmos. Environ., 38,6867–6874, doi:10.1016/j.atmosenv.2004.09.002, 2004.

Glindemann, D., Edwards, M., and Morgenstern, P.: Phosphine from rocks: Mechanically driven phosphate reduction?, Environ. Sci. Policy, 39, 8295–8299, doi:10.1021/es050682w, 2005.

Goldblatt, C. and Zahnle, K. J.: Faint young Sun paradox remains, Nature, 474, E3–E4, doi:10.1038/nature09961, 2011a.

Goldblatt, C. and Zahnle, K. J.: Clouds and the Faint Young Sun Paradox, Clim. Past, 7, 203–220, doi:10.5194/cp-7-203-2011, 2011b.

Goldblatt, C., Lenton, T. M., and Watson, A. J.: Bistability of atmospheric oxygen and the Great Oxidation, Nature, 443, 683–686, doi:10.1038/nature05169, 2006.

Goldblatt, C., Claire, M. W., Lenton, T. M., Matthews, A. J., Watson, A. J., and Zahnle, K. J.: Nitrogen-enhanced greenhouse warming on early Earth, Nat. Geosci., 2, 891–896, doi:10.1038/ngeo692, 2009.

Goody, R. and Yung, Y.: Atmospheric Radiation: Theoretical Basis, Oxford University Press, New York, USA, 1995.

Gough, D.: Solar interior structure and luminoscity variations, Sol. Phys., 74, 21–34, doi:10.1007/BF00151270, 1981.

Halevy, I., Pierrehumbert, R. T., and Schrag, D. P.: Radiative transfer in CO_2-rich paleoatmospheres, J. Geophys. Res.-Atmos., 114, D18112, doi:10.1029/2009JD011915, 2009.

Halevy, I. and Schrag, D. P.: Sulfur dioxide inhibits calcium carbonate precipitation: Implications for early Mars and Earth, Geophys. Res. Lett., 36, doi:10.1029/2009GL040792, 2009.

Hansen, J., Sato, M., Ruedy, R., Nazarenko, L., Lacis, A., Schmidt, G., Russell, G., Aleinov, I., Bauer, M., Bauer, S., Bell, N., Cairns, B., Canuto, V., Chandler, M., Cheng, Y., Del Genio, A., Faluvegi, G., Fleming, E., Friend, A., Hall, T., Jackman, C., Kelley, M., Kiang, N., Koch, D., Lean, J., Lerner, J., Lo, K., Menon, S., Miller, R., Minnis, P., Novakov, T., Oinas, V., Perlwitz, J., Perlwitz, J., Rind, D., Romanou, A., Shindell, D., Stone, P., Sun, S., Tausnev, N., Thresher, D., Wielicki, B., Wong, T., Yao, M., and Zhang, S.: Efficacy of climate forcings, J. Geophys. Res.-Atmos., 110, D18104, doi:10.1029/2005JD005776, 2005.

Haqq-Misra, J. D., Domagal-Goldman, S. D., Kasting, P. J., and Kasting, J. F.: A revised, hazy methane greenhouse for the archean earth, Astrobiology, 8, 1127–1137, doi:10.1089/ast.2007.0197, 2008.

Haqq-Misra, J., Kasting, J. F., and Lee, S.: Availability of O_2 and H_2O_2 on Pre-Photosynthetic Earth, Astrobiology, 11, 293–302, doi:10.1089/ast.2010.0572, 2011.

Harrison, J. J., Chipperfield, M. P., Dudhia, A., Cai, S., Dhomse, S., Boone, C. D., and Bernath, P. F.: Satellite observations of stratospheric carbonyl fluoride, Atmospheric Chemistry and Physics Discussions, 14, 18 127–18 180, doi:10.5194/acpd-14-18127-2014, http://www.atmos-chem-phys-discuss.net/14/18127/2014/, 2014.

Hattori, S., Danielache, S. O., Johnson, M. S., Schmidt, J. A., Kjaergaard, H. G., Toyoda, S., Ueno, Y., and Yoshida, N.: Ultraviolet absorption cross sections of carbonyl sulfide isotopologues $OC^{32}S$, $OC^{33}S$, $OC^{34}S$ and $O^{13}CS$: isotopic fractionation in photolysis and atmospheric implications, Atmos. Chem. Phys., 11, 10293–10303, doi:10.5194/acp-11-10293-2011, 2011.

Hua, W., Chen, Z. M., Jie, C. Y., Kondo, Y., Hofzumahaus, A., Takegawa, N., Chang, C. C., Lu, K. D., Miyazaki, Y., Kita, K., Wang, H. L., Zhang, Y. H., and Hu, M.: Atmospheric hydrogen peroxide and organic hydroperoxides during PRIDE-PRD'06, China: their abundance, formation mechanism and contribution to secondary aerosols, Atmos. Chem. Phys., 8, 6755–6773, 2008.

IPCC: Climate Change 2013: The Scientific Basis. Contribution of Working Group I to the Fifth Assessment Report of the Intergovernmental Panel on Climate Change, Cambridge University Press, Cambridge, UK and New York, NY, USA, 2013.

Jacob, D., Field, B., Li, Q., Blake, D., de Gouw, J., Warneke, C., Hansel, A., Wisthaler, A., Singh, H., and Guenther, A.: Global budget of methanol: Constraints from atmospheric observations, J. Geophys. Res.-Atmos., 110, doi:10.1029/2004JD005172, 2005.

Johnson, B., and Goldblatt, C.: The Nitrogen Budget of Earth, Earth-Sci. Rev., Under Review.

Johnston, H.: Global ozone balance in natural stratosphere, Rev. Geophys., 13, 637–649, doi:10.1029/RG013i005p00637, 1975.

Kasting, J. and Donahue, T.: The evolution of atmospheric ozone, J. Geophys. Res-Oc., 85, 3255–3263, doi:10.1029/JC085iC06p03255, 1980.

Kasting, J. F.: Stability of ammonia in the primitive terrestrial atmosphere, J. Geophys. Res-Oc. Atm., 87, 3091–3098, doi:10.1029/JC087iC04p03091, 1982.

Kasting, J. F., Zahnle, K. J., and Walker, J. C. G.: (1983) Photochemistry of methane in Earth's early atmosphere, Precambrian Res., 20, 121–148, doi:10.1016/0301-9268(83)90069-4, 1983.

Kasting, J. F.: Methane and climate during the Precambrian era, Precambrian Res., 137, 119–129, doi:10.1016/j.precamres.2005.03.002, 2005.

Kasting, J. F.: How was early earth kept warm?, Science, 339, 44–45, doi:10.1126/science.1232662, 2013.

Kasting, J. F., Pollack, J., and Crisp, D.: Effects of high CO_2 levels on surface-temperature and atmospheric oxidation-state of the early Earth, J. Atmos. Chem., 1, 403–428, doi:10.1007/BF00053803, 1984.

Kavanagh, L. and Goldblatt, C.: The Som Palaeobarometry Method: a critical analysis, presented at: 2012 Fall Meeting, 3–7 December, AGU, San Francisco, California, abstract P21B-1719, 2013.

Kiehl, J. and Dickinson, R.: A study of the radiative effects of enhanced atmospheric CO_2 and CH_4 on early Earth surface temperatures, J. Geophys. Res.-Atmos., 92, 2991–2998, doi:10.1029/JD092iD03p02991, 1987.

Kienert, H., Feulner, G., and Petoukhov, V.: Faint young Sun problem more severe due to ice-albedo feedback and higher rotation rate of the early Earth, Geophys. Res. Lett., 39, L23710, doi:10.1029/2012GL054381, 2012.

Kuhn, W. and Atreya, S.: Ammonia photolysis and the greenhouse effect in the primordial atmosphere of the Earth, Icarus, 37, 207–213, doi:10.1016/0019-1035(79)90126-X, 1979.

Lawler, M. J., Sander, R., Carpenter, L. J., Lee, J. D., von Glasow, R., Sommariva, R., and Saltzman, E. S.: HOCl and Cl_2 observations in marine air, Atmos. Chem. Phys., 11, 7617–7628, doi:10.5194/acp-11-7617-2011, 2011.

Lee, D., Kohler, I., Grobler, E., Rohrer, F., Sausen, R., GallardoKlenner, L., Olivier, J., Dentener, F., and Bouwman, A.: Estimations of global NOx emissions and their uncertainties, Atmos.

Environ., 31, 1735–1749, doi:10.1016/S1352-2310(96)00327-5, 1997.

Lee, C., Martin, R. V., van Donkelaar, A., Lee, H., Dickerson, R. R., Hains, J. C., Krotkov, N., Richter, A., Vinnikov, K., and Schwab, J. J.: SO_2 emissions and lifetimes: Estimates from inverse modeling using in situ and global, space-based (SCIAMACHY and OMI) observations, J. Geophys. Res.-Atmos., 116, doi:10.1029/2010JD014758, 2011.

Leue, C., Wenig, M., Wagner, T., Klimm, O., Platt, U., and Jahne, B.: Quantitative analysis of NOx emissions from Global Ozone Monitoring Experiment satellite image sequences, J. Geophys. Res.-Atmos., 106, 5493–5505, doi:10.1029/2000JD900572, 2nd AGU Chapman Conference on Water Vapor in the Climate System, POTOMAC, MD, OCT 12-15, 1999, 2001.

Li, Q., Jacob, D., Yantosca, R., Heald, C., Singh, H., Koike, M., Zhao, Y., Sachse, G., and Streets, D.: A global three-dimensional model analysis of the atmospheric budgets of HCN and CH3CN: Constraints from aircraft and ground measurements, J. Geophys. Res.-Atmos., 108, doi:10.1029/2002JD003075, 2003.

Liang, M.-C., Hartman, H., Kopp, R. E., Kirschvink, J. L., and Yung, Y. L.: Production of hydrogen peroxide in the atmosphere of a Snowball Earth and the origin of oxygenic photosynthesis, P. Natl. Acad. Sci. USA, 103, 18 896–18 899, doi:10.1073/pnas.0608839103, 2006.

Martin, R. S., Mather, T. A., and Pyle, D. M.: Volcanic emissions and the early Earth atmosphere, Geochim. Cosmochim. Ac., 71, 3673–3685, doi:10.1016/j.gca.2007.04.035, 2007.

Mather, T., Pyle, D., and Allen, A.: Volcanic source for fixed nitrogen in the early Earth's atmosphere, Geology, 32, 905–908, doi:10.1130/G20679.1, 2004.

Marty, B., Zimmermann, L., Pujol, M., Burgess, R., and Philippot, P.: Nitrogen isotopic composition and density of the archean atmosphere, Science, 342, 101–104, doi:10.1126/Science.1240971, 2013.

Meadows, V. and Crisp, D.: Ground-based near-infrared observations of the Venus nightside: the thermal structure and water abundance near the surface, J. Geophys. Res.-Planet, 101, 4595–4622, doi:10.1029/95JE03567, 1996.

Millet, D. B., Jacob, D. J., Custer, T. G., de Gouw, J. A., Goldstein, A. H., Karl, T., Singh, H. B., Sive, B. C., Talbot, R. W., Warneke, C., and Williams, J.: New constraints on terrestrial and oceanic sources of atmospheric methanol, Atmos. Chem. Phys., 8, 6887–6905, 2008.

Montzka, S. A., Calvert, P., Hall, B. D., Elkins, J. W., Conway, T. J., Tans, P. P., and Sweeney, C.: On the global distribution, seasonality, and budget of atmospheric carbonyl sulfide (COS) and some similarities to CO_2, J. Geophys. Res.-Atmos., 112, doi:10.1029/2006JD007665, 2007.

Morton, S. and Edwards, M.: Reduced phosphorus compounds in the environment, Crit. Rev. Env. Sci. Tec., 35, 333–364, doi:10.1080/10643380590944978, 2005.

Moore, R. M.: A photochemical source of methyl chloride in saline waters, Environ. Sci. Technol., 42, 1933–1937, doi:10.1021/es071920I, 2008.

Myhre, G. and Stordal, F.: Role of spatial and temporal variations in the computation of radiative forcing and GWP, J. Geophys. Res., 102, 11181–11200, doi:10.1029/97JD00148, 1997.

Navarro-Gonzalez, R., Molina, M., and Molina, L.: Nitrogen fixation by volcanic lightning in the early Earth, Geophys. Res. Lett., 25, 3123–3126, doi:10.1029/98GL02423, 1998.

Navarro-Gonzalez, R., McKay, C., and Mvondo, D.: A possible nitrogen crisis for Archaean life due to reduced nitrogen fixation by lightning, Nature, 412, 61–64, doi:10.1038/35083537, 2001.

Pavlov, A., Kasting, J., Brown, L., Rages, K., and Freedman, R.: Greenhouse warming by CH_4 in the atmosphere of early Earth, J. Geophys. Res.-Planet, 105, 11981–11990, doi:10.1029/1999JE001134, 2000.

Pavlov, A., Brown, L., and Kasting, J.: UV shielding of NH_3 and O-2 by organic hazes in the Archean atmosphere, J. Geophys. Red.-Planet, 106, 23 267–23 287, doi:10.1029/2000JE001448, 2001.

Pierrehumbert, R.: Principles of Planetary Climate, Cambridge Univ. Press, New York, 2010.

Rienecker, M. M., Suarez, M. J., Gelaro, R., Todling, R., Bacmeister, J., Liu, E., Bosilovich, M. G., Schubert, S. D., Takacs, L., Kim, G.-K., Bloom, S., Chen, J., Collins, D., Conaty, A., Da Silva, A., Gu, W., Joiner, J., Koster, R. D., Lucchesi, R., Molod, A., Owens, T., Pawson, S., Pegion, P., Redder, C. R., Reichle, R., Robertson, F. R., Ruddick, A. G., Sienkiewicz, M., and Woollen, J.: MERRA: NASA's Modern-Era Retrospective Analysis for Research and Applications, J. Climate, 24, 3624–3648, doi:10.1175/JCLI-D-11-00015.1, 2011.

Roberson, A. L., Roadt, J., Halevy, I., and Kasting, J. F.: Greenhouse warming by nitrous oxide and methane in the Proterozoic Eon, Geobiology, 9, 313–320, doi:10.1111/j.1472-4669.2011.00286.x, 2011.

Rondanelli, R. and Lindzen, R. S.: Can thin cirrus clouds in the tropics provide a solution to the faint young Sun paradox?, J. Geophys. Res., 115, D02108, doi:10.1029/2009JD012050, 2010.

Rosing, M. T., Bird, D. K., Sleep, N. H., and Bjerrum, C. J.: No climate paradox under the faint early Sun, Nature, 464, 744–747, doi:10.1038/nature08955, 2010.

Rossow, W., Zhang, Y., and Wang, J.: A statistical model of cloud vertical structure based on reconciling cloud layer amounts inferred from satellites and radiosonde humidity profiles, J. Climate, 18, 3587–3605, doi:10.1175/JCLI3479.1, 2005.

Rothman, L. S., Gordon, I. E., Barbe, A., Benner, D. C., Bernath, P. E., Birk, M., Boudon, V., Brown, L. R., Campargue, A., Champion, J. P., Chance, K., Coudert, L. H., Dana, V., Devi, V. M., Fally, S., Flaud, J. M., Gamache, R. R., Goldman, A., Jacquemart, D., Kleiner, I., Lacome, N., Lafferty, W. J., Mandin, J. Y., Massie, S. T., Mikhailenko, S. N., Miller, C. E., Moazzen-Ahmadi, N., Naumenko, O. V., Nikitin, A. V., Orphal, J., Perevalov, V. I., Perrin, A., Predoi-Cross, A., Rinsland, C. P., Rotger, M., Simeckova, M., Smith, M. A. H., Sung, K., Tashkun, S. A., Tennyson, J., Toth, R. A., Vandaele, A. C., and Vander Auwera, J.: The HITRAN 2008 molecular spectroscopic database, J. Quant. Spectrosc. Ra., 110, 533–572, doi:10.1016/j.jqsrt.2009.02.013, 2009.

Rothman, L. S., Gordon, I. E., Babikov, Y., Barbe, A., Benner, D. C., Bernath, P. F., Birk, M., Bizzocchi, L., Boudon, V., Brown, L. R., Campargue, A., Chance, K., Cohen, E. A., Coudert, L. H., Devi, V. M., Drouin, B. J., Fayt, A., Flaud, J. M., Gamache, R. R., Harrison, J. J., Hartmann, J. M., Hill, C., Hodges, J. T., Jacquemart, D., Jolly, A., Lamouroux, J., Le Roy, R. J., Li, G., Long, D. A., Lyulin, O. M., Mackie, C. J., Massie, S. T., Mikhailenko, S., Mueller, H. S. P., Nau-

menko, O. V., Nikitin, A. V., Orphal, J., Perevalov, V., Perrin, A., Polovtseva, E. R., Richard, C., Smith, M. A. H., Starikova, E., Sung, K., Tashkun, S., Tennyson, J., Toon, G. C., Tyuterev, V. G., and Wagner, G.: The HITRAN2012 molecular spectroscopic database, J. Quant. Spectrosc. Ra., 130, 4–50, doi:10.1016/j.jqsrt.2013.07.002, 2013.

Sagan, C. and Chyba, C.: The early faint sun paradox: Organic shielding of ultraviolet-labile greenhouse gases, Science, 276, 1217–1221, doi:10.1126/Science.276.5316.1217, 1997.

Sagan, C. and Mullen, G.: Earth and Mars – evolution of atmospheres and surface temperatures, Science, 177, 52–56, doi:10.1126/Science.177.4043.52, 1972.

Saikawa, E., Schlosser, C. A., and Prinn, R. G.: Global modeling of soil nitrous oxide emissions from natural processes, Global Biogeochem. Cy., 27, 972–989, doi:10.1002/gbc.20087, 2013.

Saltzman, E. S., Aydin, M., Tatum, C., and Williams, M. B.: 2,000-year record of atmospheric methyl bromide from a South Pole ice core, J. Geophys. Res.-Atmos., 113, doi:10.1029/2007JD008919, 2008.

Sawada, S. and Totsuka, T.: Natural and anthropogenic sources and fate of atmospheric ethylene, Atmos. Environ., 20, 821–832, doi:10.1016/0004-6981(86)90266-0, 1986.

Schlesinger, W. H. and Hartley, A. E.: A global budget for atmospheric ammonia, Biogeochemistry, 15, 191-211, doi:10.1007/BF00002936, 1992.

Sharpe, S., Johnson, T., Sams, R., Chu, P., Rhoderick, G., and Johnson, P.: Gas-phase databases for quantitative infrared spectroscopy, Appl. Spectrosc., 58, 1452–1461, doi:10.1366/0003702042641281, 2004.

Shaviv, N.: Toward a solution to the early faint Sun paradox: a lower cosmic ray flux from a stronger solar wind, J. Geophys. Res.-Space, 108, 1437, doi:10.1029/2003JA009997, 2003.

Sheldon, N.: Precambrian paleosols and atmospheric CO_2 levels, Precambrian Res., 147, 148–155, doi:10.1016/j.precamres.2006.02.004, 2006.

Smith, S., Pitcher, H., and Wigley, T.: Global and regional anthropogenic sulfur dioxide emissions, Global Planet. Change, 29, 99–119, doi:10.1016/S0921-8181(00)00057-6, 2001.

Som, S. M., Catling, D. C., Harnmeijer, J. P., Polivka, P. M., and Buick, R.: Air density 2.7 billion years ago limited to less than twice modern levels by fossil raindrop imprints, Nature, 484, 359–362, doi:10.1038/nature10890, 2012.

Svensen, H., Planke, S., Polozov, A. G., Schmidbauer, N., Corfu, F., Podladchikov, Y. Y., and Jamtveit, B.: Siberian gas venting and the end-Permian environmental crisis, Earth Planet Sc. Lett., 277, 490–500, doi:10.1016/j.epsl.2008.11.015, 2009.

Tian, F., Kasting, J. F., and Zahnle, K.: Revisiting HCN formation in Earth's early atmosphere, Earth Planet Sc. Lett., 308, 417–423, doi:10.1016/j.epsl.2011.06.011, 2011.

Trainer, M. G., Pavlov, A. A., Curtis, D. B., McKay, C. P., Worsnop, D. R., Delia, A. E., Toohey, D. W., Toon, O. B., and Tolbert, M. A.: Haze aerosols in the atmosphere of early Earth: Manna from Heaven, Astrobiology, 4, 409–419, doi:10.1089/ast.2004.4.409, 2004.

Trainer, M. G., Pavlov, A. A., DeWitt, H. L., Jimenez, J. L., McKay, C. P., Toon, O. B., and Tolbert, M. A.: Organic haze on Titan and the early Earth, P. Natl. Acad. Sci. USA, 103, 18 035–18 042, doi:10.1073/pnas.0608561103, 2006.

Ueno, Y., Johnson, M. S., Danielache, S. O., Eskebjerg, C., Pandey, A., and Yoshida, N.: Geological sulfur isotopes indicate elevated OCS in the Archean atmosphere, solving faint young sun paradox, P. Natl. Acad. Sci. USA, 106, 14784–14789, doi:10.1073/pnas.0903518106, 2009.

United States Environmental Protection Agency (USEPA): Methane and Nitrous Oxide Emissions From Natural Sources (EPA 430-R-10-001), Retrieved from http://www.epa.gov/outreach/pdfs/Methane-and-Nitrous-Oxide-Emissions-From-Natural-Sources.pdf, 2010.

Ussiri, D. and Lal, R.: Soil emission of nitrous oxide and its mitigation, Springer, 2012.

Verhulst, K. R., Aydin, M., and Saltzman, E. S.: Methyl chloride variability in the Taylor Dome ice core during the Holocene, J. Geophys. Res.-Atmos., 118, 12 218–12 228, doi:10.1002/2013JD020197, 2013.

von Paris, P., Rauer, H., Grenfell, J. L., Patzer, B., Hedelt, P., Stracke, B., Trautmann, T., and Schreier, F.: Warming the early earth – CO_2 reconsidered, Planet Space Sci., 56, 1244–1259, doi:10.1016/j.pss.2008.04.008, 2008.

Walker, J., Hays, P., and Kasting, J.: A negative feedback mechanism for the longterm stabilization of Earth's surface temperature, J. Geophys. Res.-Oceans, 86, 9776–9782, doi:10.1029/JC086iC10p09776, 1981.

Warneck, P.: Chemistry of the Natural Atmosphere, pp. 426–441, Academic, San Diego, Calif., 1988..

Wen, J., Pinto, J., and Yung, Y.: Photochemistry of CO and H_2O - Analysis of laboratory experiments and application to the prebiotic Earth's atmosphere, J. Geophys. Res.-Atmos., 94, 14 957–14 970, doi:10.1029/JD094iD12p14957, 1989.

Williams, M. B., Aydin, M., Tatum, C., and Saltzman, E. S.: A 2000 year atmospheric history of methyl chloride from a South Pole ice core: Evidence for climate-controlled variability, Geophys. Res. Lett., 34, doi:10.1029/2006GL029142, 2007.

WMO (World Meteorological Organization): Scientific Assessment of Ozone Depletion: 2010, Global Ozone Research and Monitoring Project-Report No. 52, WMO, Geneva, Switzerland, 2011.

Wolf, E. T. and Toon, O. B.: Hospitable archean climates simulated by a general circulation model, Astrobiology, 13, 656–673, doi:10.1089/ast.2012.0936, 2013.

Wordsworth, R., Forget, F., and Eymet, V.: Infrared collision-induced and far-line absorption in dense CO_2 atmospheres, Icarus, 210, 992–997, doi:10.1016/j.Icarus.2010.06.010, 2010.

Wordsworth, R., and Pierrehumbert, R.: Hydrogen-nitrogen greenhouse warming in Earth's early atmosphere , Science, 339, 64–67, doi: 10.1126/science.1225759, 2013.

Xiao, Y., Jacob, D. J., and Turquety, S.: Atmospheric acetylene and its relationship with CO as an indicator of air mass age, J. Geophys. Res.-Atmos., 112, doi:10.1029/2006JD008268, 2007.

Xiao, Y., Logan, J. A., Jacob, D. J., Hudman, R. C., Yantosca, R., and Blake, D. R.: Global budget of ethane and regional constraints on US sources, J. Geophys. Res.-Atmos., 113, doi:10.1029/2007JD009415, 2008.

Xin, J., Cui, J., Niu, J., Hua, S., Xia, C., Li, S., and Zhu, L.: Production of methanol from methane by methanotrophic bacteria, Biocatal. Biotransfor., 22, 225–229, doi:10.1080/10242420412331283305, 2004.

Young, G.: The geologic record of glaciation – relevance to the climatic history of Earth, Geosci. Can., 18, 100–108, 1991.

Zahnle, K.: Photochemistry of methane and the formation of hydrocyanic acid (HCN) in the earth's early atmosphere, J. Geophys. Res., 91, 2819–2834, doi:10.1029/JD091iD02p02819, 1986.

Zahnle, K., Claire, M., and Catling, D.: The loss of mass-independent fractionation in sulfur due to a Palaeoproterozoic collapse of atmospheric methane, Geobiology, 4, 271–283, doi:10.1111/j.1472-4669.2006.00085.x, 2006.

Zeng, G., Wood, S. W., Morgenstern, O., Jones, N. B., Robinson, J., and Smale, D.: Trends and variations in CO, C_2H_6, and HCN in the Southern Hemisphere point to the declining anthropogenic emissions of CO and C_2H_6, Atmos. Chem. Phys., 12, 7543–7555, doi:10.5194/acp-12-7543-2012, 2012.

Zerkle, A. L., Claire, M., Domagal-Goldman, S. D., Farquhar, J., and Poulton, S. W.: A bistable organic-rich atmosphere on the Neoarchaean Earth, Nat. Geosci., 5, 359–363, doi:10.1038/NGEO1425, 2012.

Table 1: *Global Atmospheric Budget of 20 strongest HITRAN gases.* The sources, sinks, lifetimes and concentrations of these gases are given for the modern atmosphere. Relevant literature for the Archean is reviewed.

Gas	Modern F = Flux $(\mathrm{moles/yr})$ x = Abundance (n_{gas}/n_0) τ = Atmospheric lifetime	Modern Natural Sources and Sinks	Notes for Archean
CH_3OH (methanol)	F = 2.3×10^{12}–1.5×10^{13} [1, 2] x = 10^{-9}–10^{-8} (boundary layer) 10^{-10}–10^{-9} (free troposphere)[1] τ = 5–12 days[1]	Largest known sources are plant growth and decay (chemical and enzymatic demethylation of methoxy groups)[1]. The ocean biosphere may also be a significant source[2]. The main sink is oxidation by OH[1], although, deposition[1] and possibly ocean uptake[2] are important.	Photolysis of H_2O in the presence of CO leads to the production of CH_3OH [3]. Atmospheric modelling suggests this could have produced surface abundances of $\approx 2\times10^{-13}$ in the Archean[4]. Methanotrophs produce methanol as an intermediate product which is then oxidized via formaldehyde and formate to carbon dioxide, however, it has been found that high levels of CO_2 can partially inhibit methanol oxidation[5].
HNO_3 (nitric acid)	F = unknown? x = variable τ = 2.6 hours[6]	Major sources are denitrification and lightning[6]. Lightning strikes produced NO from O_2 and N_2, which is oxidized to NO_2 and then to HNO_3. Major sinks are deposition and dilution[6].	Early Earth volcanism may have produced $\approx 10^9$–10^{10} mol/yr of fixed nitrogen compared to $\approx 10^9$ mol/year today[7]. Without atmospheric O_2, the nitrogen fixation efficiency of lightning is significantly reduced compared to today[8]. Although, it has also been suggested that nitrogen fixation by volcanic lightning could have produced 3.3×10^{10}–3.3×10^{11} mol/yr of NO (4 Gyr Ago)[9]. However, in reduced atmospheres NO reacts to form HNO (K. Zahnle, private communication).
COF_2 (carbonyl fluoride)	F = unknown? x = 10^{-10}–10^{-9} (mid atmosphere)[10] $< 10^{-10}$ (troposphere)[10] $\tau = \approx$ 3.8 years[10]	Produced in the stratosphere from photolysis of chlorofluorocarbons[11].	The vast majority of atmospheric fluorine emissions come in the form of man-made emissions[10]

H_2O_2 (hydrogen peroxide)	F = unknown x = 10^{-10}–10^{-9} [12] τ = a few days[12]	No significant direct emissions have been found. Formed by bimolecular and termolecular recombination of HO_2 and radicals during the day time[13]. Sinks include washout, dry deposition, photolysis and reactions with OH[13].	H_2O photolysis produces H_2O_2. It has been estimated that this process could produce tropospheric abundances of $\leq 1.7\times10^{-15}$ [14]. During intense glaciation higher abundances of $\approx 10^{-10}$ may have been sustained by H_2O photolysis[15]
CH_3Br (methyl bromide), (bromomethane)	F = 1×10^9 [16] x = $\approx 5\times10^{-12}$ (pre-industrial)[17] τ = 0.8 years[16]	Major natural sources are oceans, freshwater wetlands and coastal salt marshes, though other sources may be important[16]. Major sinks include oceans, oxidation by OH, photolysis, and soil microbial uptake[16].	Early Earth volcanism may have produced greater fluxes of bromine than today (10^8-10^9 mol/year of Br[17]). Siberian trap volcanism may have produced large CH_3Br fluxes (2×10^{10}–5.3×10^{10} mol/year)[18]
SO_2 (sulphur dioxide)	F = 1.2×10^{12} [19] x = variable τ = 8–78 hours[20]	Major sources are dimethyl sulphide (DMS) related (75 %) and from volcanoes (25 %)[19]. Major sinks are OH, dry deposition aerosol scavenging, and conversion to H_2SO_4.	Emergence of continents and subaerial volcanism may have resulted in much increased SO_2 emissions in the late Archean compared to the early Archean[21]. Estimates of SO_2 released by Archean volcanism are as high as $\approx 3\times10^{12}$ mol/year[22]. Modelling results suggest that $\approx 10^{-10}$ of SO_2 could have existed in the Archean atmosphere if volcanism emitted $\approx 1\times10^{12}$ mol/year[23]. It has been suggested that SO_2 abundances must have remained relatively low during the Earth's history as high abundances would have inhibited calcium carbonate precipitation[24].

NH_3 (ammonia)	F = 1.3×10^{12} [6], 5.4×10^{12} [25] x = 6.7×10^{-10} (combined NH_3 and NH_4)[6] τ = 1–5 days[26]	Sources are through biological fixation[6]. Specific sources are domesticated animals ($\approx 43\%$), sea surface ($\approx 17\%$), undisturbed soils ($\approx 13\%$), fertilizers ($\approx 12\%$), biomass burning ($\approx 7\%$), and others ($\approx 8\%$)[25]. Deposition is the largest sink[6]. Specific sinks are wet deposition on land ($\approx 53\%$), wet deposition on sea surface ($\approx 28\%$), dry deposition on land ($\approx 18\%$) and reaction with OH ($\approx 2\%$)[25].	NH_3 could have been generated by hydrolysis of HCN in the stratosphere[27]. Although even with UV shielding by an organic haze abundances greater than seem 10^{-9} unlikely[28]. Large biological flux would be possible in absence of nitrification. See section **??**
O_3 (ozone)	F = not emitted directly x = 10^{-9}–10^{-8} (troposphere)[29], $\approx 10^{-5}$ (stratosphere)[30] τ = 22 days (troposphere)	Chapman cycle: stratospheric O_3 is produced by O_2 photochemistry and is destroyed by reactions with atomic oxygen[30].	With very low atmospheric O_2 abundances, O_3 abundances would be negligible[31].
C_2H_2 (acetylene)	F = 1×10^{11} [32]–2.5×10^{11} [33] x = 10^{-12}–10^{-9} [33] τ = 2 weeks[33]	Anthropogenic sources dominate: biomass burning, natural gas loss and biofuel consumption. Oxidation by OH is a major sink.	Methane photochemistry may have sustained tropospheric abundances of $\approx 2\times10^{-14}$ in the Archean (for CH_4 and CO_2 abundances of 10^{-3}) [34]
HCOOH (formic acid)	F = 1.2×10^{12} [35] x = 3×10^{-11}–5×10^{-9} (rural)[35] τ = 1-10 days[35]	Major natural sources are bimass burning, soil, vegetation, as well as secondary production from gas-phase and aqueous photochemistry[35]. Very soluble and the major sink is thought to be deposition. Relatively long-lived with respect to oxidation by OH (25 days)[35].	

CH_3Cl (methyl chloride), (chloromethane)	F = 7.2×10^{10}-9.2×10^{10} [16] x = 4.5×10^{-10} [36] τ = 1 year	Natural sources are biomass burning and oceans[16]. a mechanism to produce CH_3Cl through the photochemical reaction of dissolved organic matter in saline waters has also been reported[37]. Major sinks include oxidation by OH, reaction with chlorine radicals, uptake by oceans and soils, and loss to the stratosphere (for tropospheric CH_3Cl)[16]	Early Earth volcanism may have produced greater fluxes of chlorine than today (10^8-10^{10} mol/year of Cl[17]). Siberian trap volcanism may have produced large CH_3Cl fluxes (2×10^{12}–5.5×10^{12} mol/year)[18]. CH_3Cl has been found to correlate very well with methane during the holocene (11–0 kyr B.P.) and appears to correlate during the last glacial period (50–30 kyr B.P.)[38]
HCN (hydrogen cyanide)	F = 5.6×10^{10}-1.3×10^{11} [39] x = $\approx 2\times10^{-10}$ [40] τ = 5.3 months (troposphere)[40]	Biomass Burning is a major source[39]. Ocean uptake, oxidation by OH, photolysis, and scavenging by precipitation are major sinks.	Upper atmospheric chemistry between CH_4 photolysis products and atomic nitrogen may have produced elevated abundances in the Archean[27, 41]. Perhaps sustaining tropospheric abundances of 10^{-8}–10^{-7} and higher abundances in the stratosphere[41]. HCN could be produced by lightning in a reduced atmosphere with $pCH_4 \geq pCO_2$ (K. Zahnle, private communication).
PH_3 (phosphine)	F = unknown x = $< 10^{-13}$ (free troposphere)[42] τ = 28 hours[43]	Possible sources are Lightning and microbes[44]. The main sink is reaction with OH producing phosphate which returns to the surface in rain[43].	Simulated lightning in a methane model atmosphere has been shown to reduce phosphate to PH_3 [44]. Production of phosphine from posphate may also be produced via tectonic forces and processing of rocks[45].
C_2H_4 (Ethylene)	F = 3×10^{10} x = 10^{-11}–10^{-8} [46] τ = a few days[46]	Major sources are plants and microorganisms. Destroyed by OH ($\approx 90\%$) and O_3($\approx 10\%$) [46].	Methane photochemistry may have sustained tropospheric abundances of $\approx 2\times10^{-13}$ in the Archean (for CH_4 and CO_2 abundances of 10^{-3}) [34]

OCS (Carbonyl sulfide)	F = 1×10^{9}-3.3×10^{10} [47] x = 5×10^{-10} [47] τ = 1.5-3 years[47],4.3 years[48]	Major sources are oceanic emissions, oxidation of oceanic CS_2 and DMS, and biomass burning. Major sinks are uptake by vegetation and soils, and OH oxidation. OCS is oxidized in the stratosphere to form sulphate particles which influence the radiative budget[47].	abundances of 5×10^{-6} have been suggested in the Archean[49]. However, other have found that abundances above 10^{-8} appear unlikely due to rapid OCS photolysis[50] [23]. See section **??**
HOCl (hypochlorous acid)	F = unknown? x = 5×10^{-12}–1.7×10^{-10} [51] τ = days?	Cl can form HOCl via gas phase reactions[21].	Early Earth volcanism may have produced greater fluxes of chlorine than today (10^{8}-10^{10} mol/year of Cl[17]).
N_2O (nitrous oxide)	F = 8.6×10^{11} [52] x = 2.7×10^{-7} [53] τ = 131 years[53]	Produced as an intermediate product of both nitrification and denitrification[52]. Primary natural sources are upland soils and riparian areas, oceans, estuaries, and rivers[52]. Destroyed by chemical reactions in the upper atmosphere.	It has been proposed that large amounts of N_2O could have been produced in the Proterozoic due to bacterial denitrification in copper depleted water[54]. However, it has been shown that N_2O would be rapidly photodissociated if O_2 levels were lower than 0.1 PAL[55].
NO_2 (nitrogen dioxide)	F = 7×10^{11}-3.6×10^{12} [56] x = 3×10^{-10} (NO,NO_2, and NO_3) [6] τ = 27 hours[56]	Lightning, Biomass Burning, and soils are main sources[57]. Lightning strikes produced NO from O_2 and N_2, which is oxidized to NO_2. a major sink is dry deposition[6].	Early Earth volcanism may have produced $\approx10^{9}$–10^{10} mol/yr of fixed nitrogen compared to $\approx10^{9}$ mol/year today[7]. Without O_2, the nitrogen fixation efficiency of lightning is significantly reduced compared to today[8]. Although, it has also been suggested that nitrogen fixation by volcanic lightning could have produced 3.3×10^{10}–3.3×10^{11} mol/yr of NO (4 Gyr Ago)[9]. However, in reduced atmospheres NO reacts to form HNO (K. Zahnle, private communication).
C_2H_6 (ethane)	F = 2.0×10^{11} [32] x = 10^{-10}–5×10^{-9} [58] τ = 2 months[58]	Anthropogenic sources dominate: biomass burning, natural gas loss and biofuel consumption. Oxidation by OH is a major sink.	Methane photochemistry may have sustained tropospheric abundances of $\approx5\times10^{-6}$ in the Archean (for CH_4 and CO_2 abundances of 10^{-3})[34]. See section **??**

[1] Jacob et al. (2005) and references within. [2] Millet et al. (2008) [3] Bar-Nun and Chang (1983) [4] Wen et al. (1989) [5] Xin et al. (2004) [6] Ussiri and Lal (2012) [7] Mather et al. (2004) [8] Navarro-Gonzalez et al. (2001) [9] Navarro-Gonzalez et al. (1998) [10] Harrison et al. (2014) [11] Duchatelet et al. (2009) [12] Allen et al. (2013) [13] Hua et al. (2008) [14] Haqq-Misra et al. (2011) [15] Liang et al. (2006) [16] WMO (2011) [17] Martin et al. (2007) [18] Svensen et al. (2009) [19] Smith et al. (2001) [20] Lee et al. (2011) [21] Gaillard et al. (2011) [22] Zahnle et al. (2006) [23] Zerkle et al. (2012) [24] Halevy et al. (2009) [25] Schlesinger and Hartley (1992) [26] Warneck (1988) [27] Zahnle (1986) [28] Pavlov et al. (2001) [29] Fishman and Crutzen (1978) [30] Johnston (1975) [31] Kasting and Donahue (1980) [32] Abad et al. (2011) [33] Xiao et al. (2007) [34] Haqq-Misra et al. (2008) [35] Chebbi and Carlier (1996) [36] Williams et al. (2007) [37] Moore (2008) [38] Verhulst et al. (2013) [39] Zeng et al. (2012) [40] Li et al. (2003) [41] Tian et al. (2011) [42] Glindemann et al. (2003) [43] Morton and Edwards (2005) [44] Glindemann et al. (2004) [45] Glindemann et al. (2005) [46] Sawada and Totsuka (1986) [47] **?** and Montzka et al. (2007) [48] Chin and Davis (1995) [49] Ueno et al. (2009) [50] Domagal-Goldman et al. (2011) [51] Lawler et al. (2011) [52] USEPA (2010) [53] IPCC (2013) [54] Buick (2007) [55] Roberson et al. (2011) [56] Leue et al. (2001) [57] Lee et al. (1997) [58] Xiao et al. (2008)

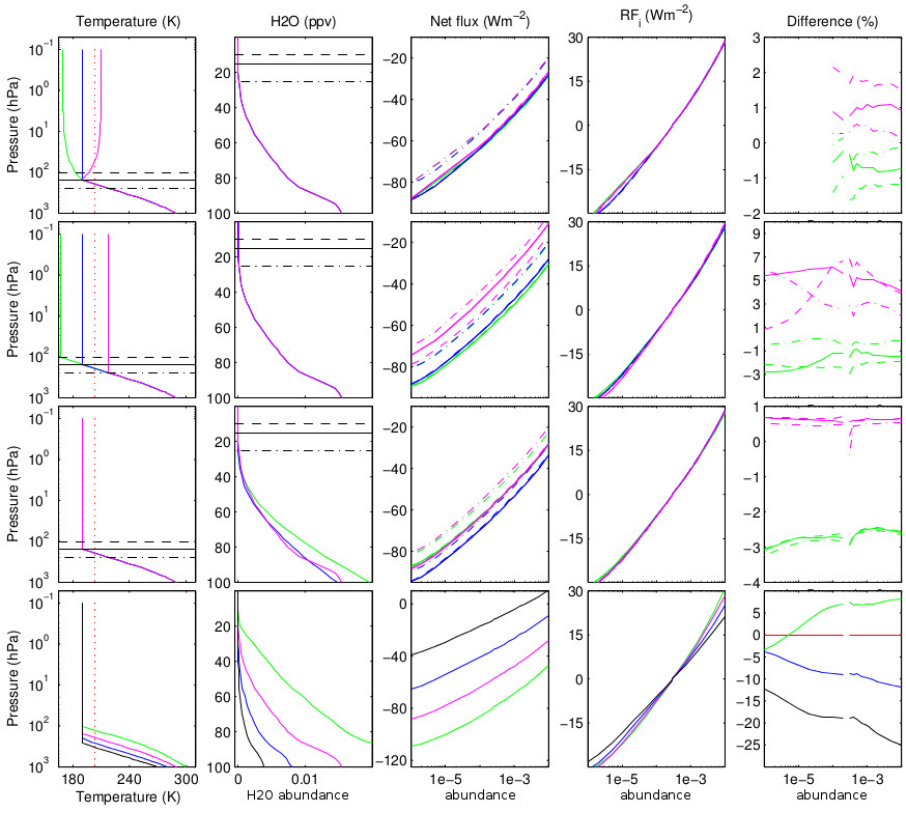

Figure A1. *Sensitivity Study.* Columns from left to right: Temperature structure, H_2O structure, Net flux of radiation at tropopause, radiative forcing, and percentage difference in radiative forcing. Solid, dashed and dashed-dotted curves represent different tropopause positions. Vertical dotted red line shows the atmospheric skin temperature (203 K).